TRE ALTAMIRA
A CLS Group Company

EXECUTIVE REPORT

Monitoring of bridge deformation using InSAR - Historical study

Client:

Ministeries van de Vlaamse Gemeenschap
Departement Mobiliteit en Openbare Werken - Afdeling Geotechniek

Reference:

Title:	Monitoring of bridge deformation using InSAR – Historical study
TRE ALTAMIRA Project Reference:	JO22-1877-ES
TRE ALTAMIRA Delivery Reference:	ES7659A007S / E765975A006S / ES7659A004E / ES7659A003V / ES7659A005S

Prepared by:

TRE ALTAMIRA

Author:	Eric Henrion, Pablo Blanco, Jordi Sanchez, Thomas Montanaro
Verified by:	Ségolène Duprat
Approved by:	Stefano Cespa
Date:	December 23
Version:	1.0

List of document modifications

Version	Date	Sections	List of modification
01.0	20/12/2022	All	Creation of the document
02.0	20/12/2023	1 ; 4.1 ; 4.2 ; 4.3 ; 4.4 ; 5.2 ; 5.4 ; 5.6 ; 8 ; 9	Update of the document

Table of Contents

Acronyms and Abbreviations

AOI	Area of Interest
ATS	Average Time Series
DEM	Digital Elevation Model
DS	Distributed Scatterer
GIS	Geographic Information System
InSAR	Interferometric Synthetic Aperture Radar
LOS	Line of Sight
PS	Permanent Scatterer
SAR	Synthetic Aperture Radar
SNT	Sentinel-1 satellite
SqueeSAR®	The most recent InSAR algorithm patented by TRE
TS	Time Series
TSX	TerraSAR-X satellite

Table of Illustrations

1. Introduction

The Flemish public administration (Department of Mobility and Public Works / Geotechnics Division) manages more than 2 500 bridges. Using this innovative contract, it wants to monitor surface displacements with InSAR (Interferometric Synthetic Aperture Radar) analysis and to prove the added value compared to the current method used for monitoring bridge deformation (via levelling). A total of **457** infrastructures are monitored in the scope of this project through a detailed analysis, out of a total of **1336** simplified infrastructures not analysed but included in the processing.

These bridges and their surroundings will be analysed using Sentinel-1 (SNT) SAR satellites in ascending and descending geometries, TerraSAR-X (TSX) SAR satellite in descending geometry, and the patented SqueeSAR® algorithm to provide the state of the art of surface ground movements. The SNT images cover the period from February 2015 to June 2022, and the TSX images cover the period from June 20214 to March 2016. A 2D decomposition (vertical and horizontal components) is carried out using the results from both SNT geometries.

In addition to deformation and deformation rates from each study, further analysis will be carried out over the bridges to extract all available information about their behaviour.

- **Maximum availability of results in case of works and in-depth analysis of zone where no InSAR points are available**: this analysis is based on amplitude images to allow the client to analyse any correlation between construction work and measurement point availability.
- **Surroundings**: this analysis is based on the height estimation of measurement points to identify which ones are on the bridge and which are not.
- **Automation of longitudinal profiles**: this analysis generates deformation profiles superimposed to a bridge sketch.
- **Detection of sudden changes in displacement**: this analysis is based on Trend Variation analysis on the measurement point time series to detect abnormal behaviour.
- **Temperature variations**: this analysis estimates a thermal dilation model from the temperature record and retrieves the thermal component from the measurement point time series.
- **Alerting system**: this analysis is based on a polygon-based approach using the shapefiles of the bridges colour-coded with the surface deformations corrected from their thermal component.

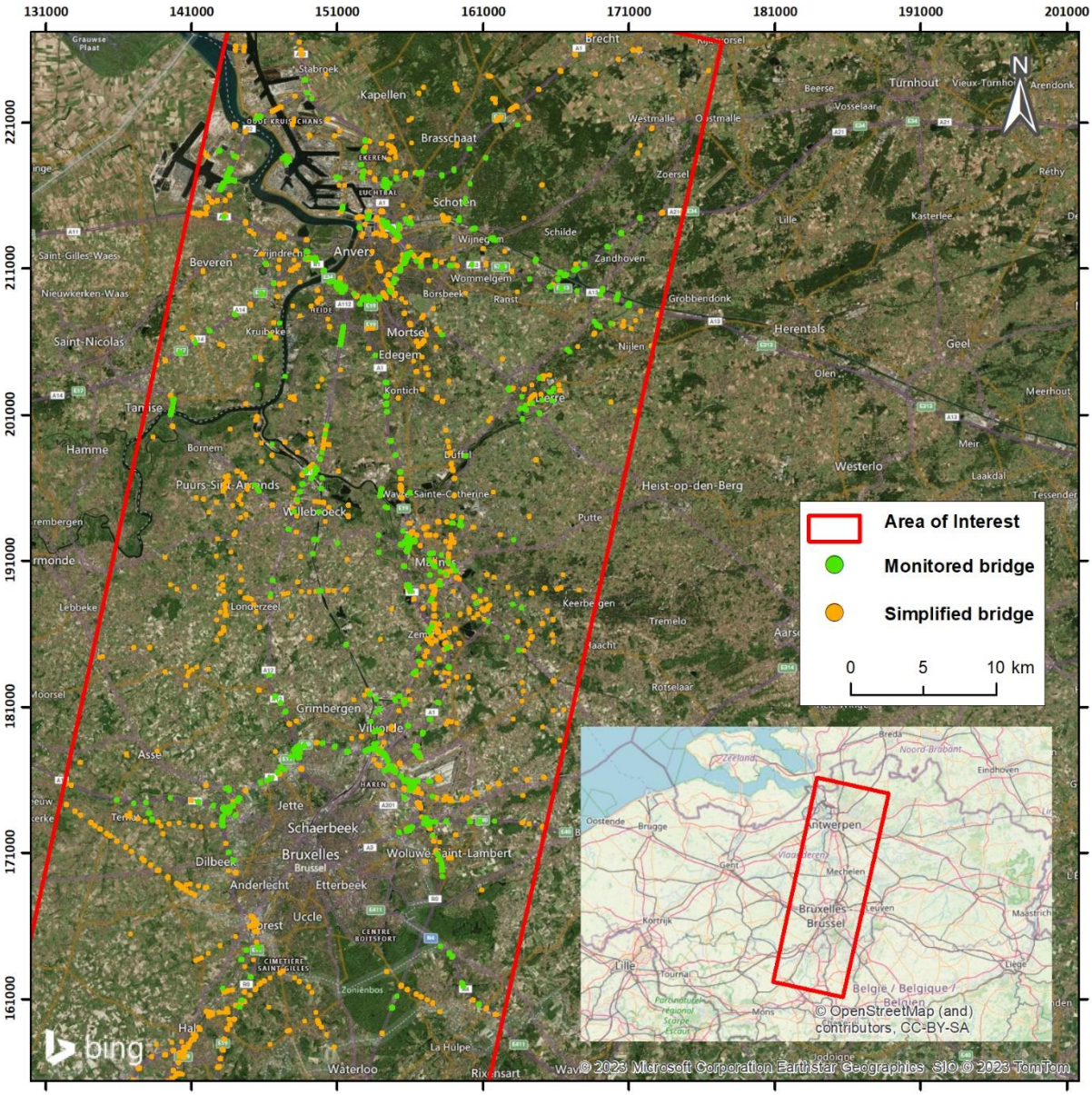

Figure 1. Area Of Interest (in red), the bridge locations are represented by green (detailed) and orange (simplified) circles.

2. InSAR principles

SqueeSAR® is the advanced multi-image InSAR algorithm patented by TRE Altamira that provides high-precision measurements of ground displacements in the form of a point cloud. By analysing a stack of SAR images acquired over a site, the SqueeSAR® algorithm identifies and measures the movement of radar reflectors on the ground surface that remain visible and coherent throughout the period of the analysis.

Radar reflectors belong to two different families (Figure 2):

- **Permanent Scatterers (PS):** point-wise radar targets characterised by highly stable radar signal returns (e.g., buildings, rocky outcrops, infrastructures, etc.)
- **Distributed Scatterers (DS):** patches of ground exhibiting a lower but homogenous radar signal return (e.g., rangeland, debris fields, arid areas, etc.). DS are represented as individual points, but the information does not refer to a single target, but rather to the patch of ground associated with each DS (the size in [km²] is provided but not the exact shape of the patch).

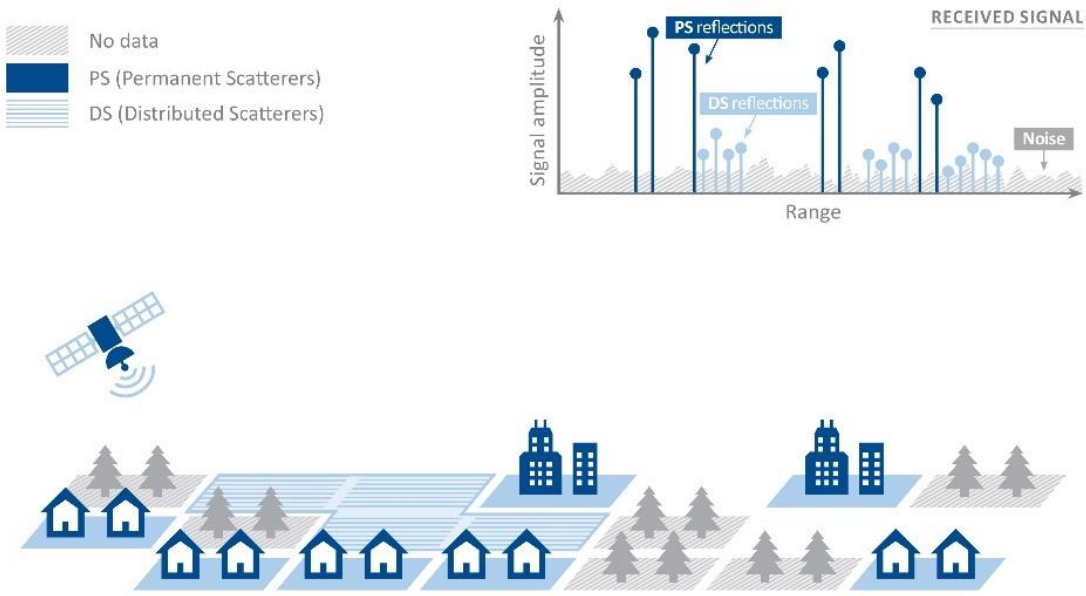

Figure 2: Schematic of PS and DS radar targets.

The density and distribution of MPs identified by the analysis are related to the resolution of the images and the surface characteristics of the area. In general, MP density increases with satellite resolution and over areas of bare ground and man-made structures and decreases with the

presence of vegetation and over areas with changes to the ground over time (e.g., snow, earthworks).

SqueeSAR® is best suited for displacement rates < 1m/yr. It provides 1D measurements (section 2.1) along the satellite Line-Of-Sight (LOS), which corresponds to the projection of the true displacement vector onto the LOS. SqueeSAR® measurements are differential in space and time:

- spatially, they are related to a local reference point (REF);
- and temporally, to the date of the first available satellite image.

The REF is assumed to be motionless and selected for its radar properties to optimise the quality of the measurements. It corresponds to a radar target with a high interferometric coherence signal in all the archive images and is not affected by displacement rate variations (non-linear movement or cyclical deformation) in the analysis period. The selection of the REF is imagery-dependent. If the imagery changes (number of images and/or time span), the MP selected as the REF can change. Furthermore, the geographic location of the chosen MP as REF is not considered. However, the absolute movement of the REF point can be defined only with calibration to a GNSS network.

For each measurement point (MP), the SqueeSAR® algorithm provides the following main information:

- Position and elevation estimated with respect to the input DEM [m];
- Displacement time series (TS) representing the evolution of the displacement for each acquisition date [mm] and measured along the LOS direction;
- Annual average displacement rate [mm/yr], calculated from a linear regression of the displacement time series over the analysis period and referred to the REF.

2.1. 1D Measurements

As InSAR measures the projection of the true displacement vector onto the LOS, the sign and value of the SqueeSAR® measurement depend on the orientation of the real displacement with respect to the LOS (Figure 3).

The LOS deformation rates are calculated from a linear regression of the ground movement measured over the entire period covered by the satellite images. Each measurement point corresponds to a Permanent Scatterer (PS) or a Distributed Scatterer (DS), colour-coded according to its annual rate of movement and direction. For example, in a descending LOS analysis, negative values (red) indicate surface deformation away from the satellite (i.e., subsidence and/or westward movement), while positive values (blue) indicate surface deformation towards the satellite (i.e., uplift and/or eastward movement). And in an ascending LOS analysis, negative values (red) indicate

movement away from the satellite (i.e., subsidence and/or eastward movement), while positive values (blue) indicate movement towards the satellite (i.e., uplift and/or westward movement).

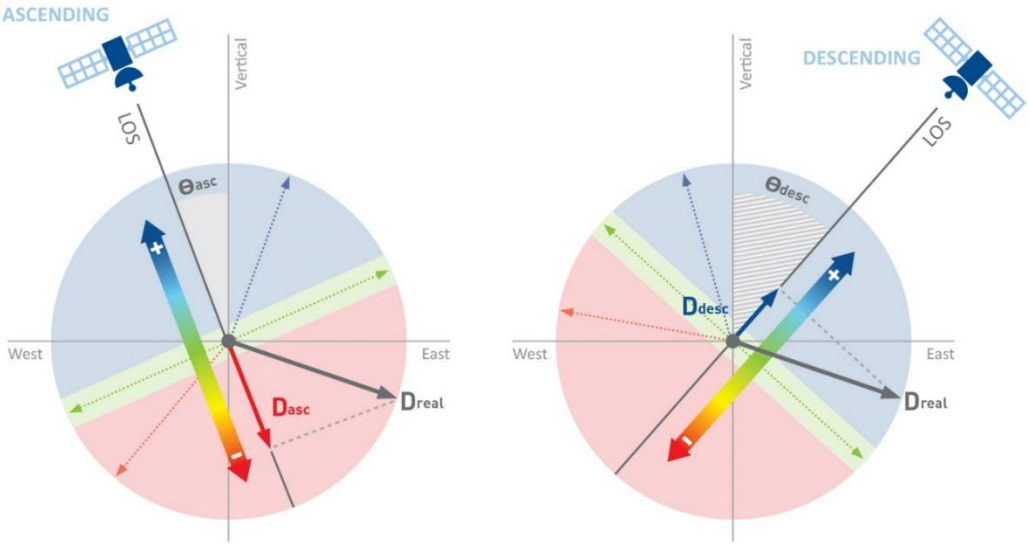

Figure 3: SqueeSAR measures real movement (Dreal) projection onto the LOS. The same real movement (Dreal) produces a different value from a different LOS (different inclination or different orbits). Real displacement vectors (Dreal) within the blue areas will produce positive LOS measurements, while those within the red areas will produce negative LOS values. Real displacement vectors within the green band (i.e., perpendicular to the satellite LOS) will produce small (i.e., close to zero) LOS measurements.

2.2. 2D Measurements

Combining 1D (LOS) SqueeSAR® results from ascending and descending orbits over the same area and overlapping periods produces 2D (vertical and east-west) measurements.

The estimation of the 2D measurements requires the following steps and assumptions:

- Satellites travelling in ascending and descending orbits identify different radar targets on the ground, entailing that the 2D procedure requires a spatial grid to capture MPs from both orbits within each cell. It is assumed that the same motion affects MPs that fall within the same cell. All MPs within the same cell are then averaged. Note that the 2D cells do not represent radar targets on the ground but rather synthetic points located at the centre of the cells (Figure 4).
- A 2D time series is calculated by combining all ascending and descending time series using trigonometry. Only cells that contain points from both input LOS datasets will produce a 2D time series. The spatial coverage of the 2D information is thus generally lower than that of the individual LOS datasets (Figure 4).

- Since the images are acquired on different dates from each orbit, the LOS displacement time series must be resampled in time. The final output includes all ascending and descending acquisition dates and covers the overlapping period in common for the two datasets.
- North-south movement cannot be measured with InSAR as SAR satellites are not sensitive to movement parallel to their travel direction.

As in LOS analyses, average annual displacement rates in a 2D analysis are calculated from a linear regression of the displacement measured over the entire period of the study, and all measurements are relative to a reference point that is assumed to be stable.

The convention for displacement sign and point colour is the following (Figure 5):

- In a vertical dataset, negative values (from yellow to red) indicate downward displacement (subsidence), while positive values (from pale to dark blue) indicate upward displacement (uplift or heave).
- In an east-west dataset, negative values (from yellow to red) indicate westward motion, while positive values (from pale to dark blue) indicate eastward motion.

2D measurements are generally easier to interpret than LOS data, but they have a lower spatial resolution, which means that in a detailed analysis of localised features, it may be beneficial to use the full-resolution LOS results.

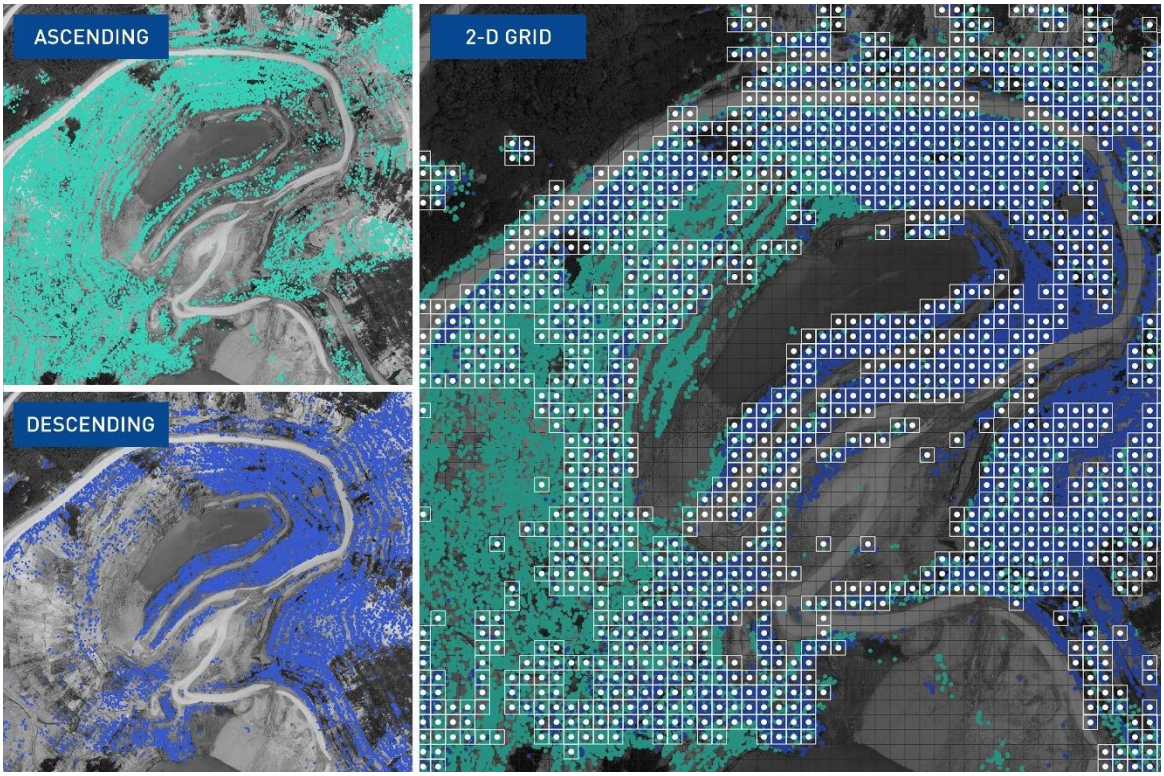

Figure 4: 2D measurements are estimated by subsampling ascending and descending data on a common spatial grid. The measurements of all MPs within the same cell are averaged to produce 2D measurement points located at the centre of the cell. The 2D procedure only produces readings for cells containing MP from both orbits (white cells).

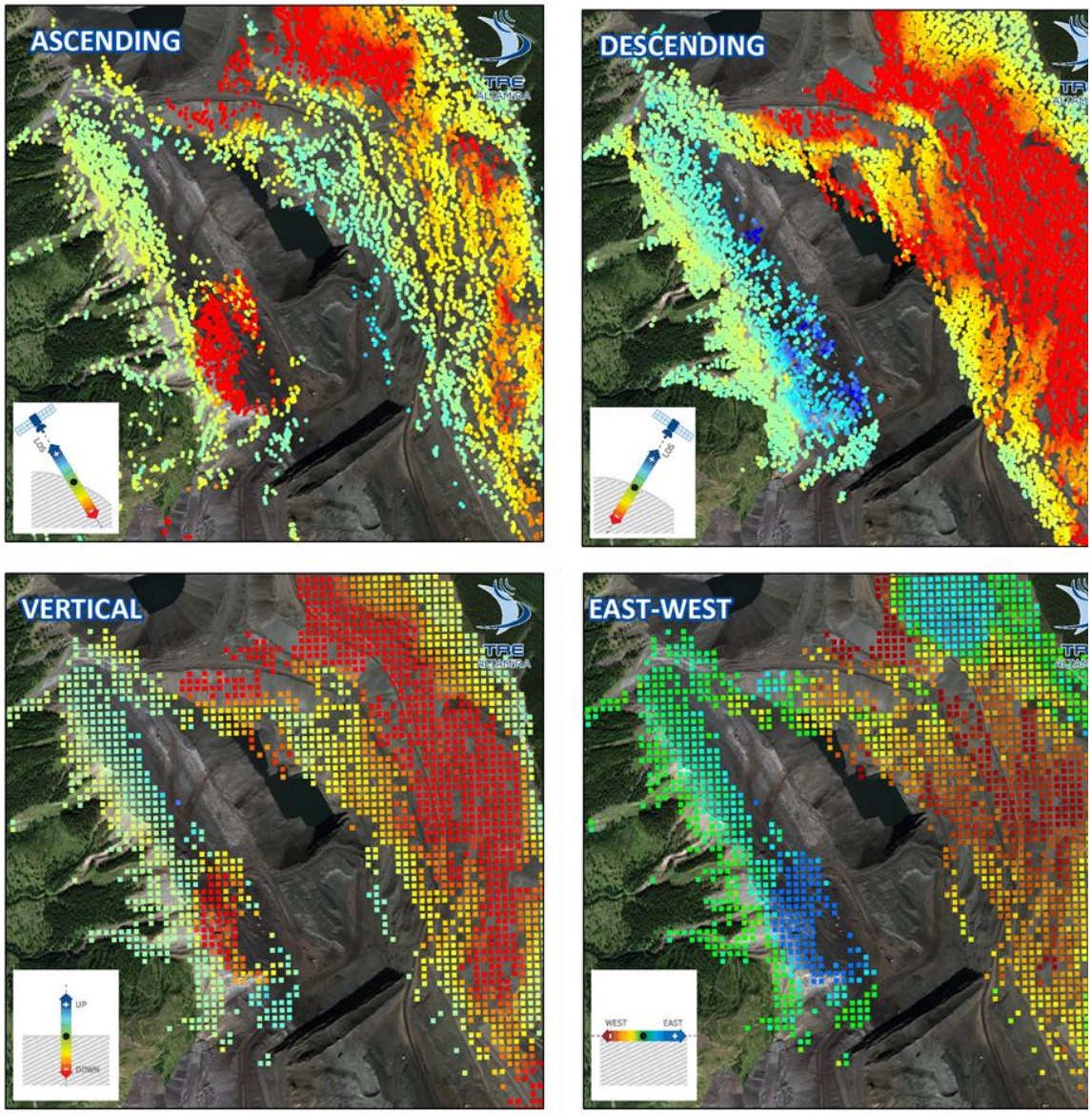

Figure 5: Ascending and descending LOS measurements correspond to the full-resolution network of natural reflectors identified on the ground and provide the projection of the real movement to the specific LOS. The combination of ascending and descending data produces a regular grid of vertical and east-west measurements.

2.3. Measurement point displacement accuracy

The precision of SqueeSAR® displacement measurements depends on performing a correct phase unwrapping and estimating the atmospheric contribution. Since the elaboration is statistically based, the main factors influencing the accuracy are not only related to the quality of each single acquisition but also the quality of the entire processed dataset.

The atmospheric noise component for each acquisition depends on the following:

- At the time of acquisition, there is a greater atmospheric noise during the daytime.
- The acquisition geometry, higher LOS angle implies a longer distance to cover and, therefore, more atmospheric disturbance.
- The distance from the reference point.

The SqueeSAR® algorithm can measure displacement with millimetre precision (Table 1). The precision depends on the quality of the imagery and the coherence of the signal. In particular, the precision:

- increases with the number of processed images, the length of the period of the analysis, the frequency of acquisitions, the coherence of the signal (i.e., the absence of vegetation or surface disturbances) and the density of points identified;
- decreases with gaps in the acquisitions, strong atmospheric disturbances, and surface variations in the analysis period (e.g., snow, floods, changes to the ground surface).

SqueeSAR® LOS measurements are provided with two displacement precision indices:

- The displacement rate standard deviation (V_STDEV) indicates the precision of the annual deformation rate with respect to the REF. Given the standard deviation (σ) and assuming that the errors are normally distributed (Gaussian), 95% of the rate values tend to be included in a ±2σ range. The displacement rate standard deviation increases with the distance of the point from the REF.
- The time series error bar (STD_DEF) indicates the precision of single displacement measurements. A single estimate is produced for each measurement point. It depends on the temporal coherence of the phase signal: the lower the error bar, the higher the coherence of the MP and the precision of the measurements. This parameter is calculated as the standard deviation of the residuals of the displacement time series with respect to an analytic model (i.e., how well the model fits the displacement time series). The model is selected individually for each measurement point with an advanced Model Order Selection technique that also considers the quality of the image archive (number of processed images, time span covered by the archive and possible gaps in the acquisitions).

Considering a dataset of at least 30 scenes covering a 2-year period, a MP located less than 1 km away from the REF had a typical standard deviation value lower than 1 mm/year. The precision of the single displacement value is, on average, within ± 5 mm (Table 1). Average precision for a single measurement in a time series is not statistically evaluated but derived from validation against ground truth.

LOS measurements	Displacement rate standard deviation	Error bar of a single measurement
Precision	±1 mm/yr	±5 mm

Table 1: Typical precision values for a MP less than 1 km from the REF and a dataset of at least 30 SAR scenes.

2.4. Geolocation accuracy

Since all InSAR measurements are relative to the REF, the MP location's absolute accuracy depends on the selected REF's location for the analysis. In general, InSAR data geocoding is refined using a priori information (i.e., an ortho-photo of the area of interest over which InSAR vector data is overlain or a set of ground control points). However, the absolute location of the REF with respect to the International Terrestrial Reference Frame (ITRF) can be verified only using an independent GNSS (Global Navigation Satellite System) site.

Nevertheless, in most applications, the relative accuracy of the target's coordinates (i.e., how well the vector between two points is estimated) is much more important than absolute accuracy. Any systematic shift can be dealt with easily; these shifts do not typically compromise data interpretation.

While the precision of the displacement measurements is millimetric, the position of individual measurement points is known with metric accuracy and depends on the satellite system being used (Table 2). As for the measurement precision, the position accuracy increases with the number of processed images, the length of the analysis period, the frequency of acquisitions, and the coherence of the signal (i.e., the absence of vegetation or surface disturbances). Table 2 reports the typical accuracy values associated with MP's UTM coordinates at mid-latitudes. Table 2 shows the specific precision values associated with satellites commonly used in operational SqueeSAR® processing.

Satellite	Band	Wavelength [cm]	Resolution RGxAZ [mxm]	North-South [m]	East-West [m]	Elevation [m]
ERS - ENVI	C-band	5.6	20x5	± 2	± 7	± 1.5
RSAT (*Standard Beam*)	C-band	5.6	20x5	± 2	± 7	± 1.5
SNT	**C-band**	**5.9**	**5x20**	**± 8**	**± 12**	**±8**
CSK	X-band	3.12	3x3	± 1	± 1	±0.5
TSX (*Stripmap*)	**X-band**	**3.11**	**3x3**	**± 1**	**± 3**	**± 1.5**
TSX (*Spotlight*)	X-band	3.11	1x1	± 0.5	± 3	± 1.5
ALOS-1 (*Fine Beam*)	L-band	23.6	16.6x16.6	± 1.5	± 3	± 2
ALOS-2 (*Fine SM3 Beam*)	L-band	23.8	10x10	± 1.5	± 3	± 2

Table 2: Typical precision values (1 sigma) associated with the UTM coordinates of a MP at mid-latitudes. Values are referred to a MP less than 1 km from the REF and a dataset of at least 30 SAR scenes (the satellites used in this study are shown in blue).

An estimation of the geolocation accuracy is provided with the SqueeSAR® results with the parameter GEO_STDEV. This parameter is derived from the spatial resolution of the SAR image and the H_STDEV parameter (accuracy of the estimated height of the MP).

2.5. Phase unwrapping and fast movements

As already mentioned, the precision of the measurements depends on performing a correct phase unwrapping. In the case of rapid deformation (construction works) affecting single isolated targets, phase unwrapping can be affected by the equivocation of the phase.

Figure 6 illustrates a schematic of the equivocation phenomena. The grey solid represents a radar system acquisition target. The target is represented at an initial R_0 distance (in blue), while three possible cases are shifted to R0 by different entities in red. Without prior information, the system cannot estimate the correct number of wavelengths (nλ) which occurred; therefore, all three cases will have equivalent ΔR shift measurements.

More precisely, it is needed to measure the displacement and the direction of motion. This means that, theoretically, on a single isolated radar target, only displacement below half a wavelength will be correctly detected. A greater displacement may be misinterpreted. In extreme cases, if the

target moved exactly half a wavelength between two acquisitions, the target would be considered perfectly stable.

These theoretical limits refer to fast movements affecting single isolated radar targets. Measurement ambiguities can be resolved in cases the movement is spatially correlated, and the MP density is adequate.

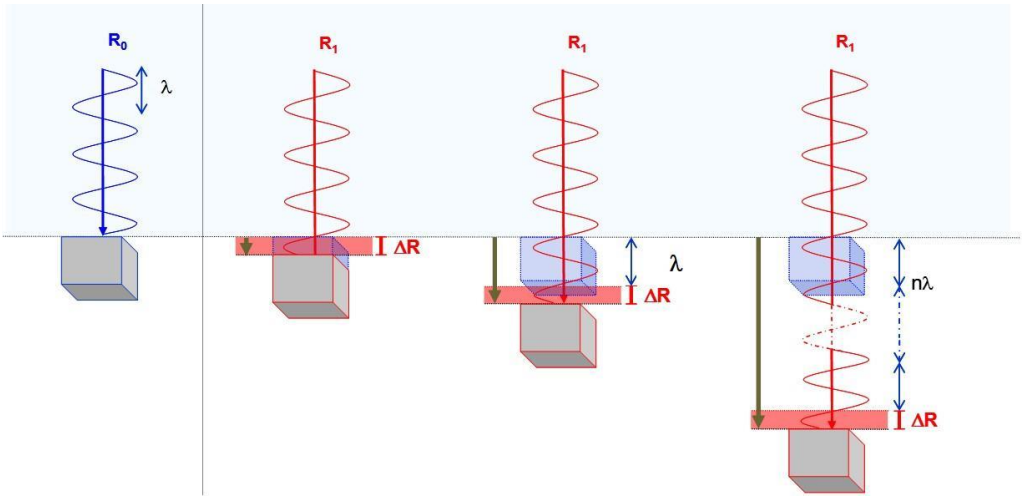

Figure 6: Schematic of a sinusoidal phase of the electromagnetic wave incident on a moving target (grey solid). Without prior information, it is impossible to estimate the correct number of wavelengths (n) that occur, and in all three cases, an equivalent ΔR shift is measured.

Figure 7 shows a schematic of a spatially correlated subsidence phenomenon. When the radar targets density is adequate, a correct phase unwrapping can be operated, and a total displacement higher than the λ/4 limit can be measured. If the radar target distribution is inadequate, an incorrect phase unwrapping can cause an underestimation of the displacement that occurred.

The temporal distribution of the acquisitions impacts the phase unwrapping correctness: the higher the acquisition frequency, the higher the ability to correctly unwrap and describe fast movements.

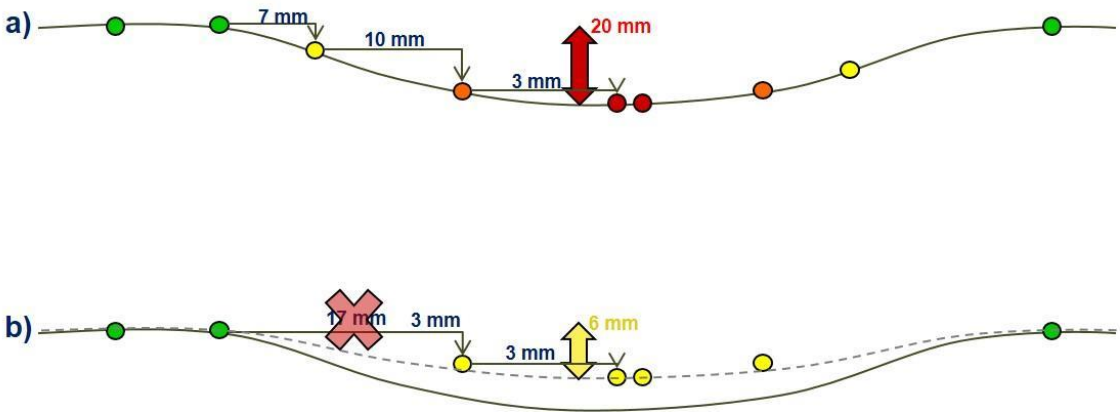

Figure 7: Schematic of a spatially correlated subsidence phenomenon. The MP are colour-coded accordingly to the displacement measured. Considering a C-band satellite, a total displacement of 20 mm (higher than the λ/4 limit of 14 mm) can be estimated when the MPs are well distributed along the subsiding profile (a). When the MP distribution is inadequate, an underestimation of the real displacement occurs (b).

3. SAR Data

The historical radar data available over the AOI consists of medium and high-resolution images acquired by the SNT (ascending and descending orbits) and TSX (descending orbit). The SNT mission is operated by the European Space Agency (ESA). It is composed of a constellation of two satellites, Sentinel-1A and Sentinel-1B, which share the same orbit and acquire in C-band (wavelength = 5.66 cm) at a ground resolution of 20 m x 5 m. The TSX mission is operated by the German Space Agency (DLR) and owned by Airbus. The TSX satellite is closely followed by its twin TanDEM-X on the same orbit, and they are backed up by the Spanish satellite PAZ. They acquire in X-band (wavelength = 3.10 cm) at a ground resolution of 3 m x 3 m.

The 374 SNT images in descending geometry cover the period from February 10th, 2015, to June 21st, 2022, with a 6-day revisit frequency (Table 3).

The 365 SNT images in ascending geometry cover the period from February 13th, 2015, to June 24th, 2022, with a 6-day revisit frequency (Table 3).

The 53 TSX images cover the period from June 13th, 2014, to March 23rd, 2016, with an 11-day revisit frequency (Table 3).

Satellite	Pixel Resolution	Orbit Geometry	Track	LOS Angle (θ)	# Images	Date Range
Sentinel-1	20 m x 5 m	Descending	110	35.86°	374	2015/02/10 – 2022/06/21
Sentinel-1	20 m x 5 m	Ascending	161	40.21	365	2015/02/13 – 2022/06/24
TerraSAR-X	3 m x 3 m	Descending	48	21.60°	53	2014/06/13 – 2016/03/23

Table 3: Satellite acquisition parameters and image acquisition information.

The temporal distribution of SNT (descending and ascending geometries) and TSX (descending geometry) images processed is shown in Figure 8.

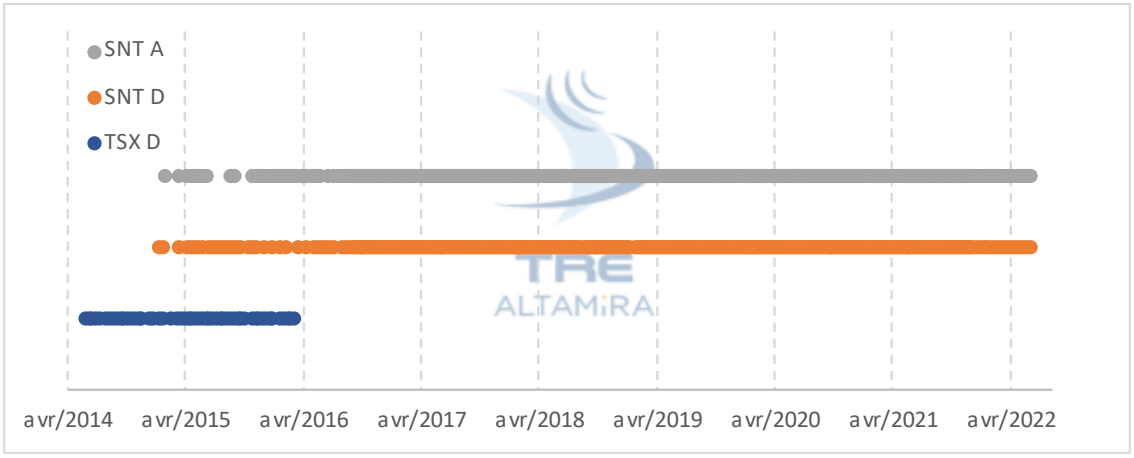

Figure 8: Temporal distribution of SNT (grey for ascending and orange for descending) and TSX (blue) images processed over the AOI.

Finally, the image acquisition characteristics for SNT and TSX satellites are given in Figure 9, Figure 10 and Figure 11 (the θ angle represents the inclination to the vertical, and the δ angle represents the inclination of the North-South axis).

Satellite info

Satellite	Wavelength	Satellite geometry	Sensor mode	Satellite track
SNT	5.55 cm	DESCENDING	IW	110

Acquisition geometry

Line of sight angle	**θ:**	35.86°	**δ:**	9.66°	
Line of sight versors	**V:**	0.81	**N:**	-0.098	**E:** 0.578

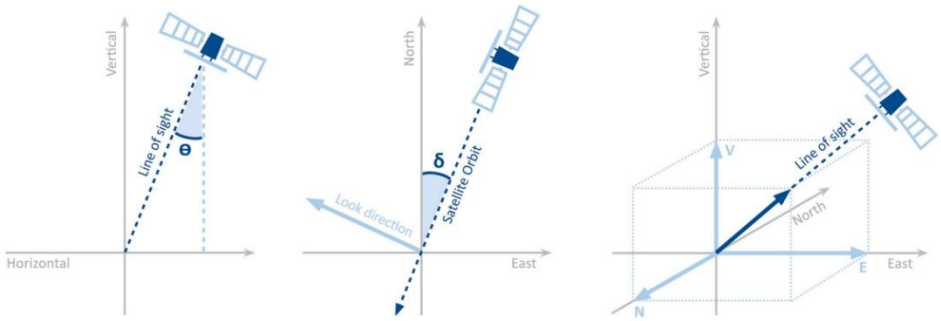

Figure 9: Acquisition geometry in descending mode for the SNT images used for the SqueeSAR® analysis.

Satellite info

Satellite	Wavelength	Satellite geometry	Sensor mode	Satellite track
SNT	5.55 cm	ASCENDING	IW	161

Acquisition geometry

Line of sight angle	**ɵ:**	40.21°	**δ:**	10.85°		
Line of sight versors	**V:**	0.764	**N:**	-0.121	**E:**	-0.634

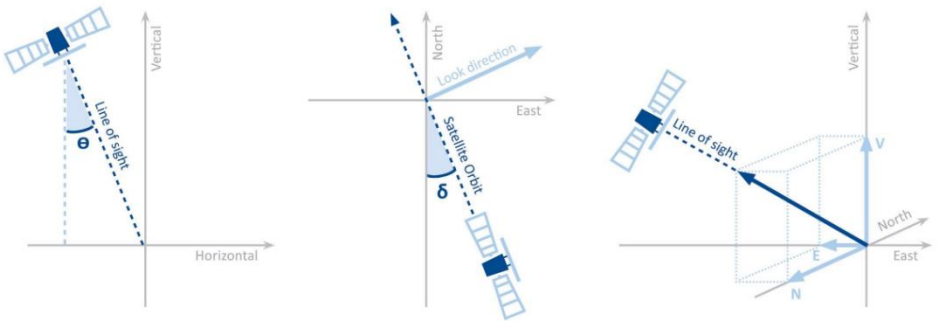

Figure 10: Acquisition geometry in ascending mode for the SNT images used for the SqueeSAR® analysis.

Satellite info

Satellite	Wavelength	Satellite geometry	Sensor mode	Satellite track
TSX	3.11 cm	DESCENDING	SM003	48

Acquisition geometry

Line of sight angle	**ɵ:**	21.6°	**δ:**	11.27°		
Line of sight versors	**V:**	0.93	**N:**	-0.072	**E:**	0.361

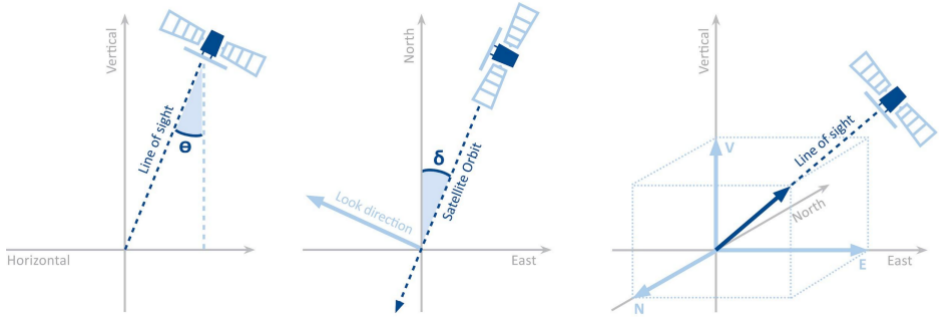

Figure 11: Acquisition geometry in descending mode for the TSX images used for the SqueeSAR® analysis.

Figure 12 represents the footprints of the SNT (ascending and descending geometries) and TSX images.

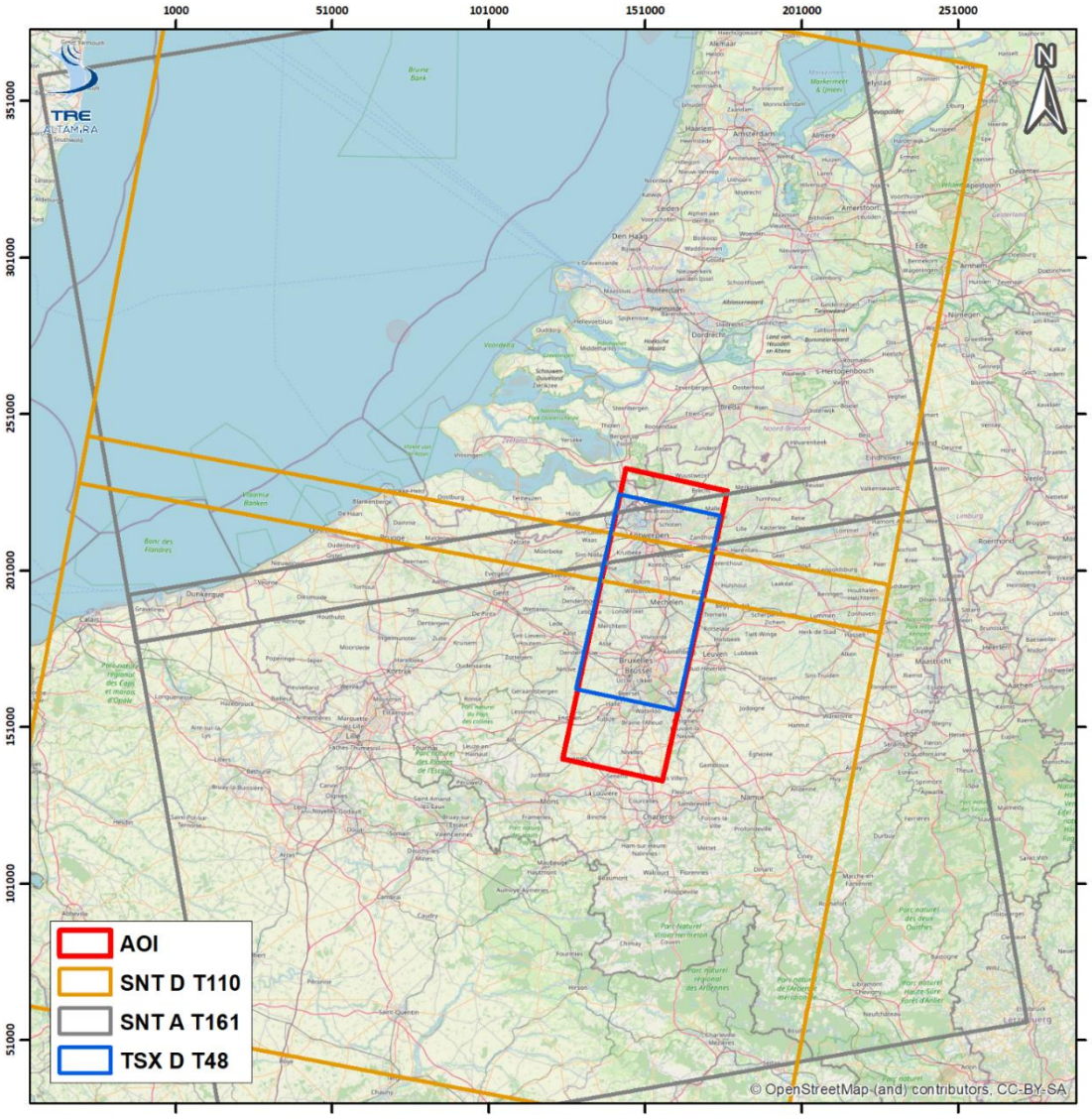

Figure 12. Area Of Interest (in red), the footprints of SNT and TSX images are represented with the corresponding colours in Figure 8.

4. Results

4.1. Reference Point

The REF coordinates related to the SNT and TSX SqueeSAR® analysis are reported in Table 4 and Table 5, respectively.

Code	Geographic coordinates (°)		Plane coordinates Lambert 72 (m)	
	Longitude	Latitude	East	North
BAZGLJM (D)	4.4331104	50.8364824	154 533.47	169 564.96
DMYRQ2A (A)	4.3523196	50.8477952	148 842.74	170 821.51

Table 4: REF location for the SNT SqueeSAR® analysis (D: descending, A: ascending).

Code	Geographic coordinates (°)		Plane coordinates Lambert 72 (m)	
	Longitude	Latitude	East	North
E3FRO7W (D)	4.3267686	51.0798661	147 057.69	196 638.84

Table 5: REF location for the TSX SqueeSAR® analysis (D: descending).

4.2. Permanent Scatterers (PS) and Distributed Scatterers (DS)

For the SNT SqueeSAR® analysis in descending geometry, 8 316 536 MP have been obtained for a spatial density of 2 660 MP/km². The statistical repartition of the nature of MPs shows a high percentage of PS due to the urban context of the study (Table 6).

Nb. of MP	Type	
	PS	DS
8 316 536	7 453 203	863 333
100 %	89.62 %	10.38 %

Table 6: Statistical repartition of MPs for the SNT SqueeSAR® analysis in descending geometry.

For the SNT SqueeSAR® analysis in ascending geometry, 9 614 837 MP have been obtained for a spatial density of 3 075 MP/km². The statistical repartition of the nature of MPs is presented in Table 7.

Nb. of MP	Type	
	PS	DS
9 614 837	8 596 213	1 018 624
100 %	89.41 %	10.59 %

Table 7: Statistical repartition of MPs for the SNT SqueeSAR® analysis in ascending geometry.

For the TSX SqueeSAR® analysis, 21 433 890 MPs have been obtained for a spatial density of 10 211 MP/km² (roughly eight times higher than the SNT studies). The statistical repartition is presented in Table 8.

Nb. of MP	Type	
	PS	DS
21 433 890	19 283 631	2 150 529
100 %	89.97 %	10.03 %

Table 8: Statistical repartition of MPs for the TSX SqueeSAR® analysis in descending geometry.

Figure 13, Figure 14, and Figure 15 show the spatial distribution of the PS and DS through the SqueeSAR® SNT descending, SNT ascending, and TSX descending analyses, respectively. The spatial distribution is similar between the three studies, with PS located in urban areas and DS predominantly located in areas with moderate vegetation or agricultural fields.

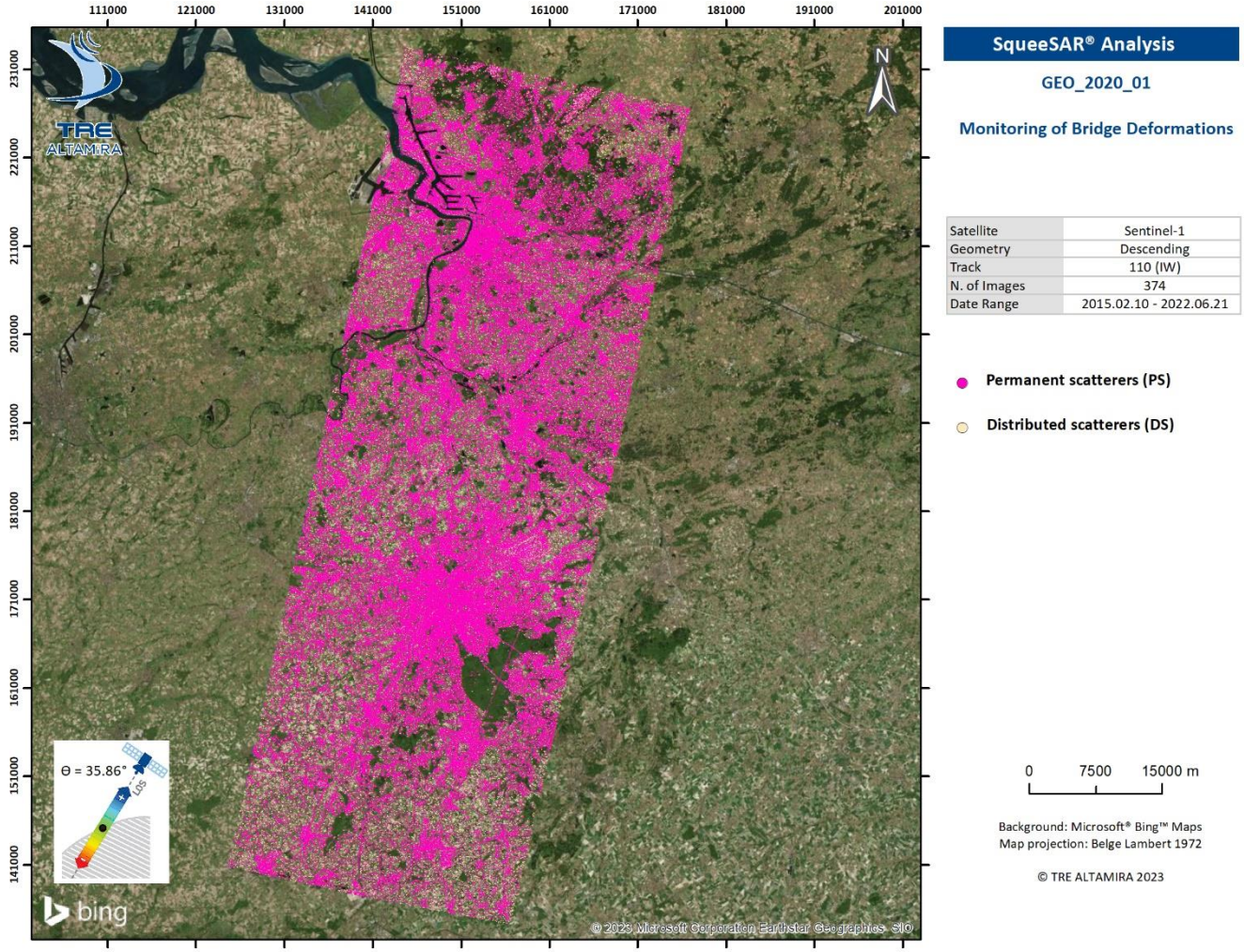

Figure 13. Spatial distribution of the PS and DS through the SNT SqueeSAR® results in descending geometry.

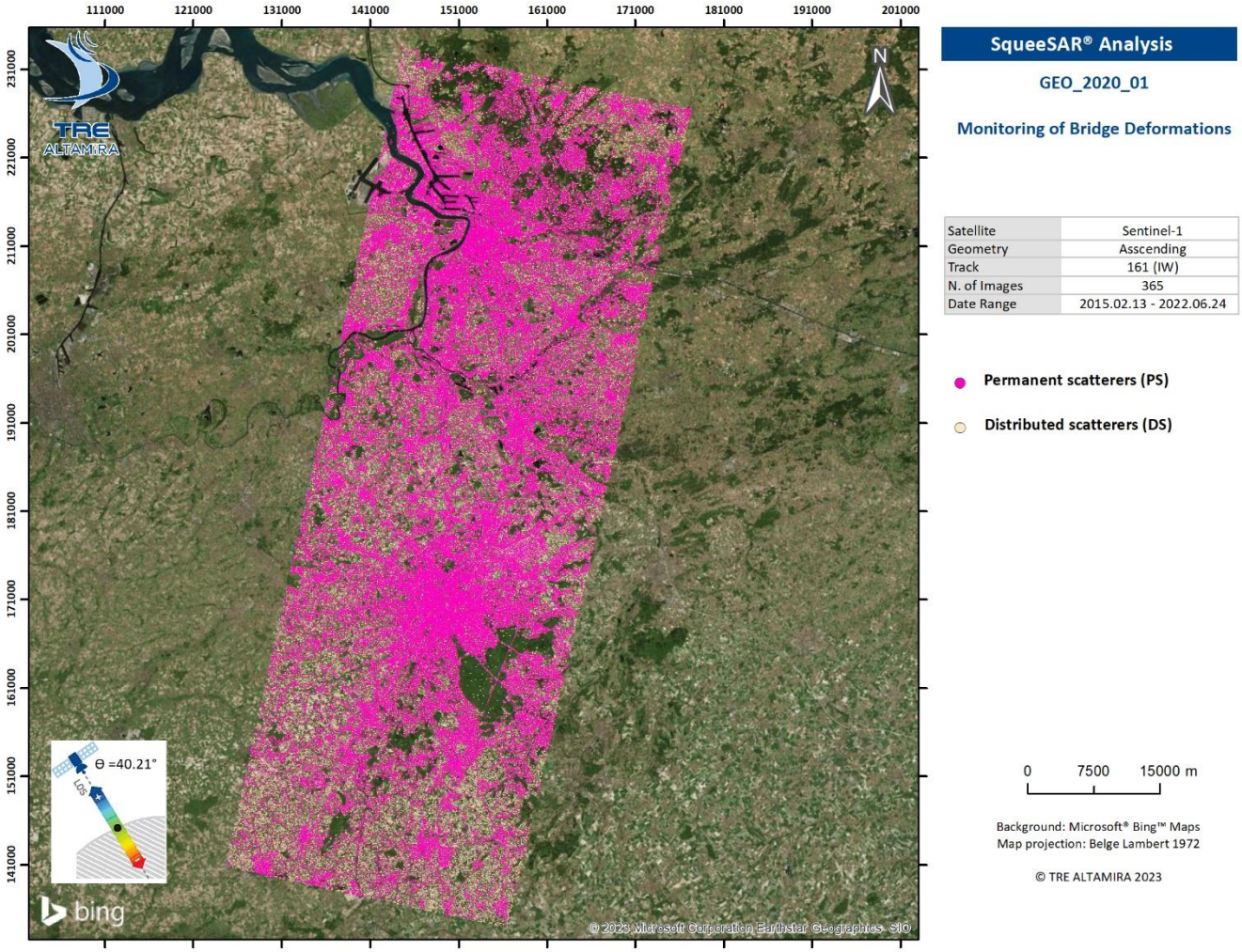

Figure 14. Spatial distribution of the PS and DS through the SNT SqueeSAR® results in ascending geometry.

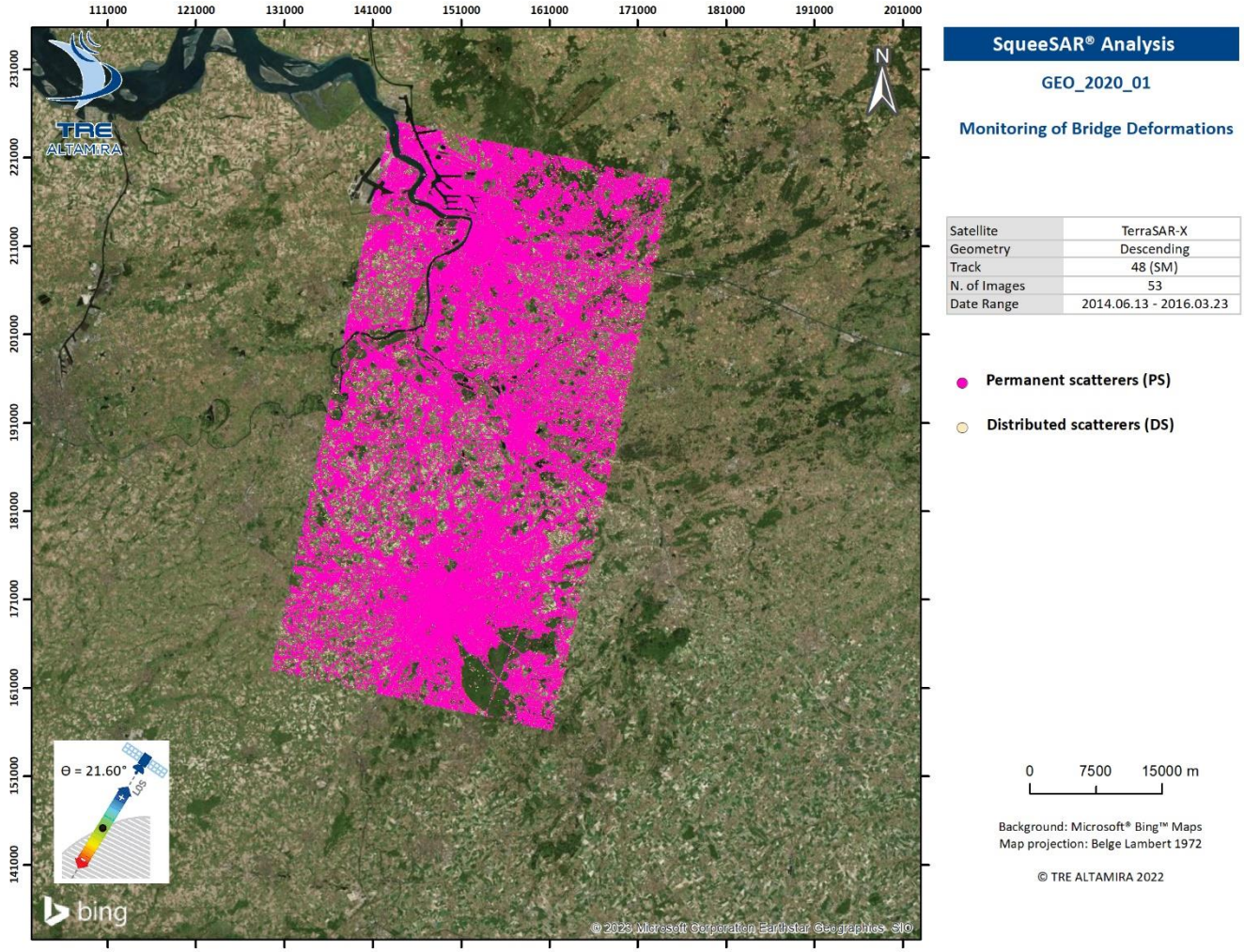

Figure 15. Spatial distribution of the PS and DS through the TSX SqueeSAR® results in descending geometry.

4.3. Deformation rates and deformation maps

The LOS deformation rates measured in millimetres per year from the SNT descending archive are shown in Figure 16. The deformation rate ranges from -93 mm/yr to 35 mm/yr with a mean value of -1 mm/yr and a standard deviation of ± 4 mm/yr (Figure 16).

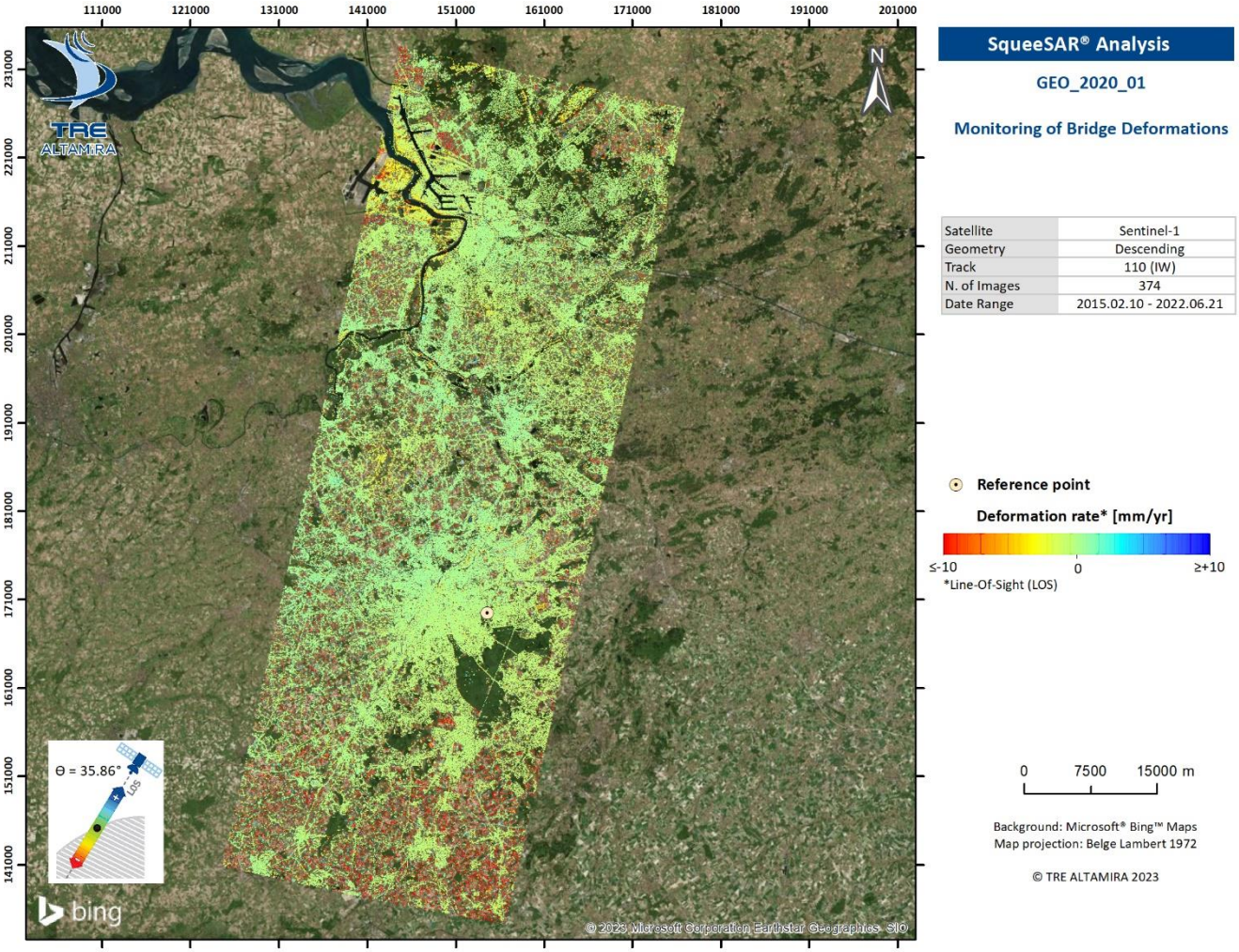

Figure 16: LOS deformation rate from the descending geometry of SNT SqueeSAR® analysis.

The LOS deformation measured in millimetres from the SNT descending is shown in Figure 17. The deformation ranges from -655 mm to 254 mm with a mean value of -6 mm and a standard deviation of ± 32 mm (Figure 17).

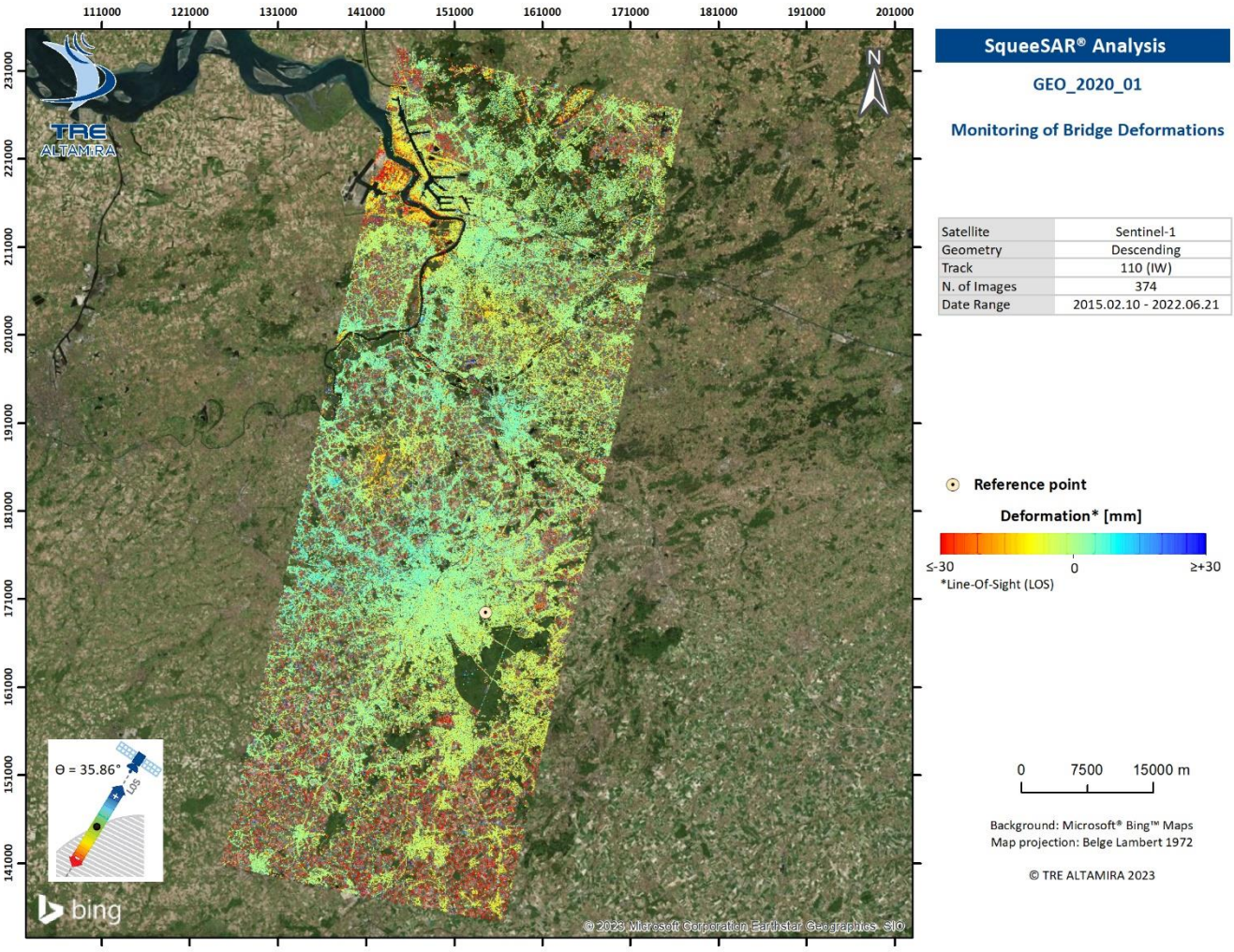

Figure 17: LOS deformation from the descending geometry of SNT SqueeSAR® analysis.

The LOS deformation rates measured in millimetres per year from the SNT ascending archive are shown in Figure 18. The deformation rate ranges from -93 mm/yr to 39 mm/yr with a mean value of -2 mm/yr and a standard deviation of ± 7 mm/yr (Figure 18).

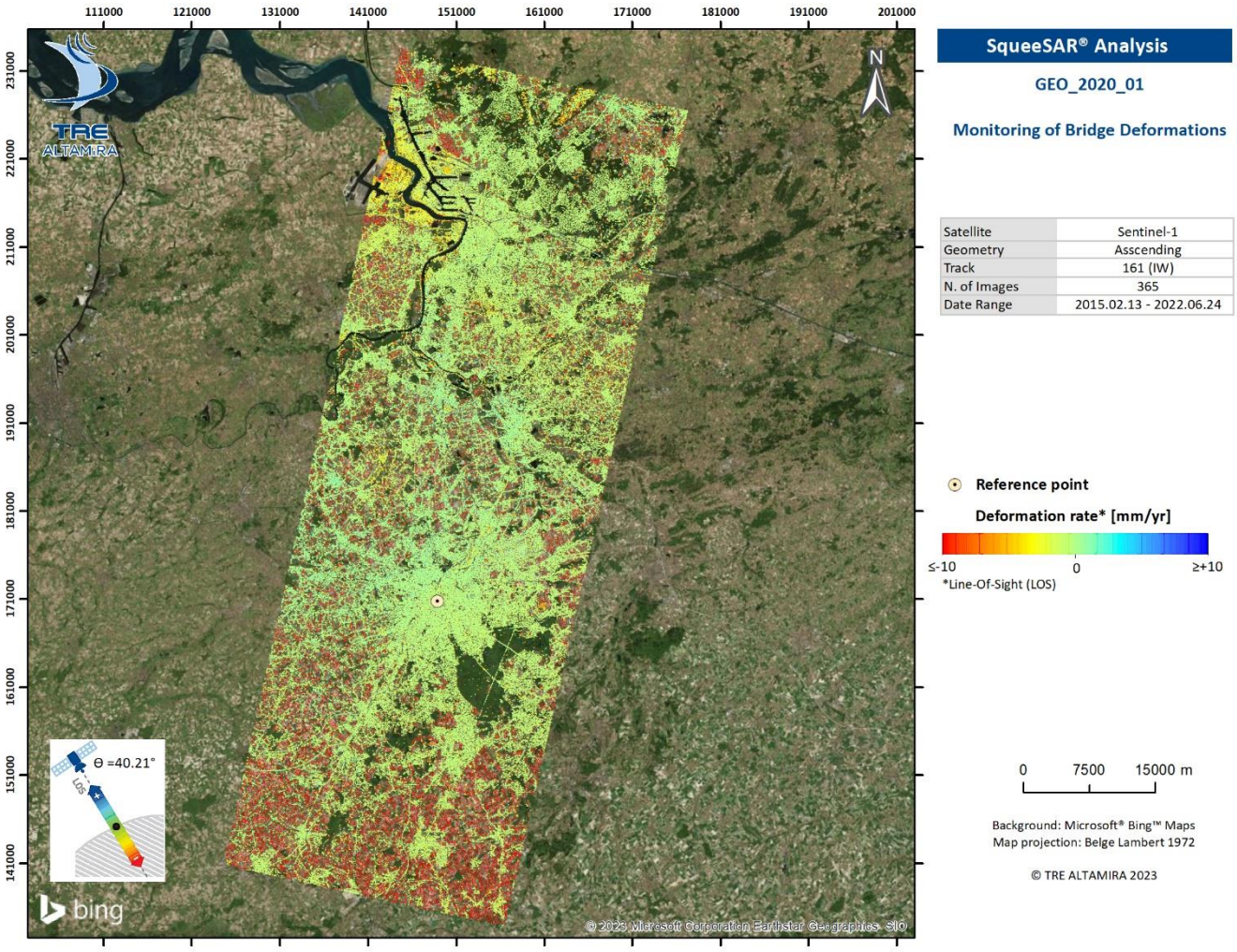

Figure 18: LOS deformation rate from the ascending geometry of SNT SqueeSAR® analysis.

The LOS deformation measured in millimetres from the SNT ascending is shown in Figure 19. The deformation ranges from -674 mm to 334 mm with a mean value of -16 mm and a standard deviation of ± 51 mm (Figure 19).

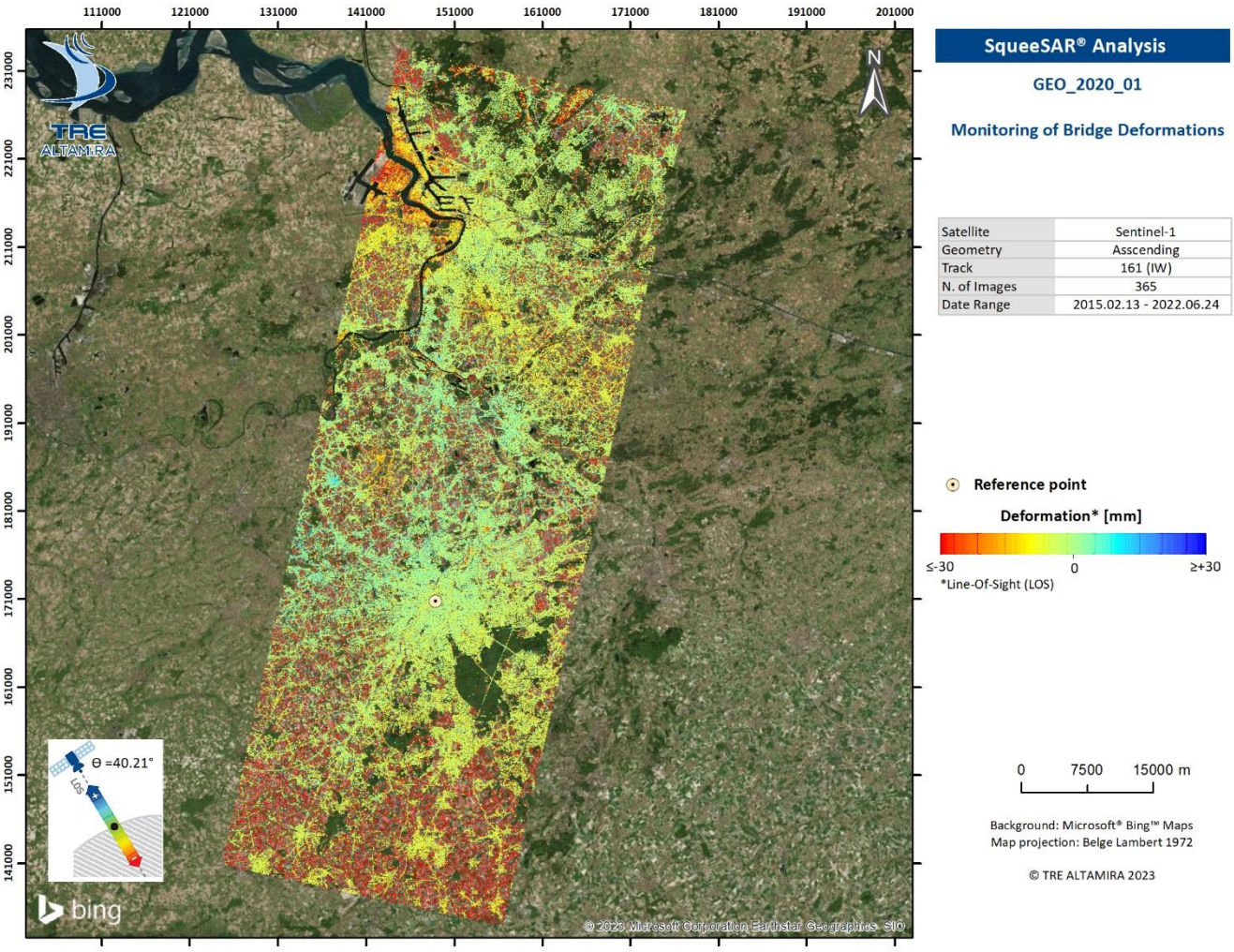

Figure 19: LOS deformation from the ascending geometry of SNT SqueeSAR® analysis.

The vertical deformation rate in millimetres per year from the SNT descending and ascending archives (2D decomposition) is shown in Figure 20. The deformation rate ranges from -112 mm/yr to 33 mm/yr with a mean value of -4 mm/yr and a standard deviation of ± 9 mm/yr (Figure 20).

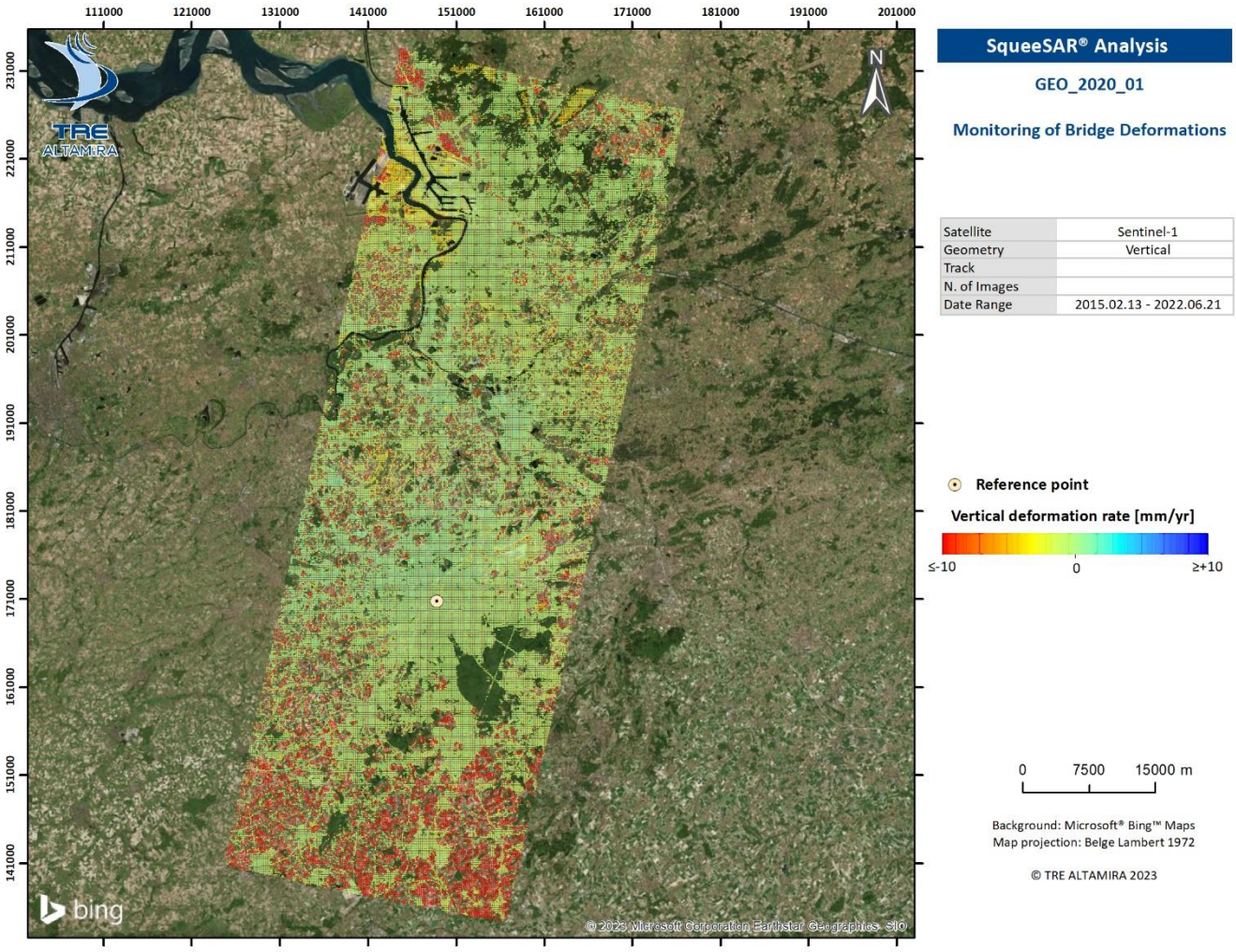

Figure 20: Vertical deformation rate from the descending and ascending geometries (2D decomposition) of SNT SqueeSAR® analysis.

The vertical deformation in millimetres from the SNT descending and ascending archives (2D decomposition) is shown in Figure 21. The deformation ranges from -790 mm to 249 mm with a mean value of -29 mm and a standard deviation of ± 64 mm (Figure 21).

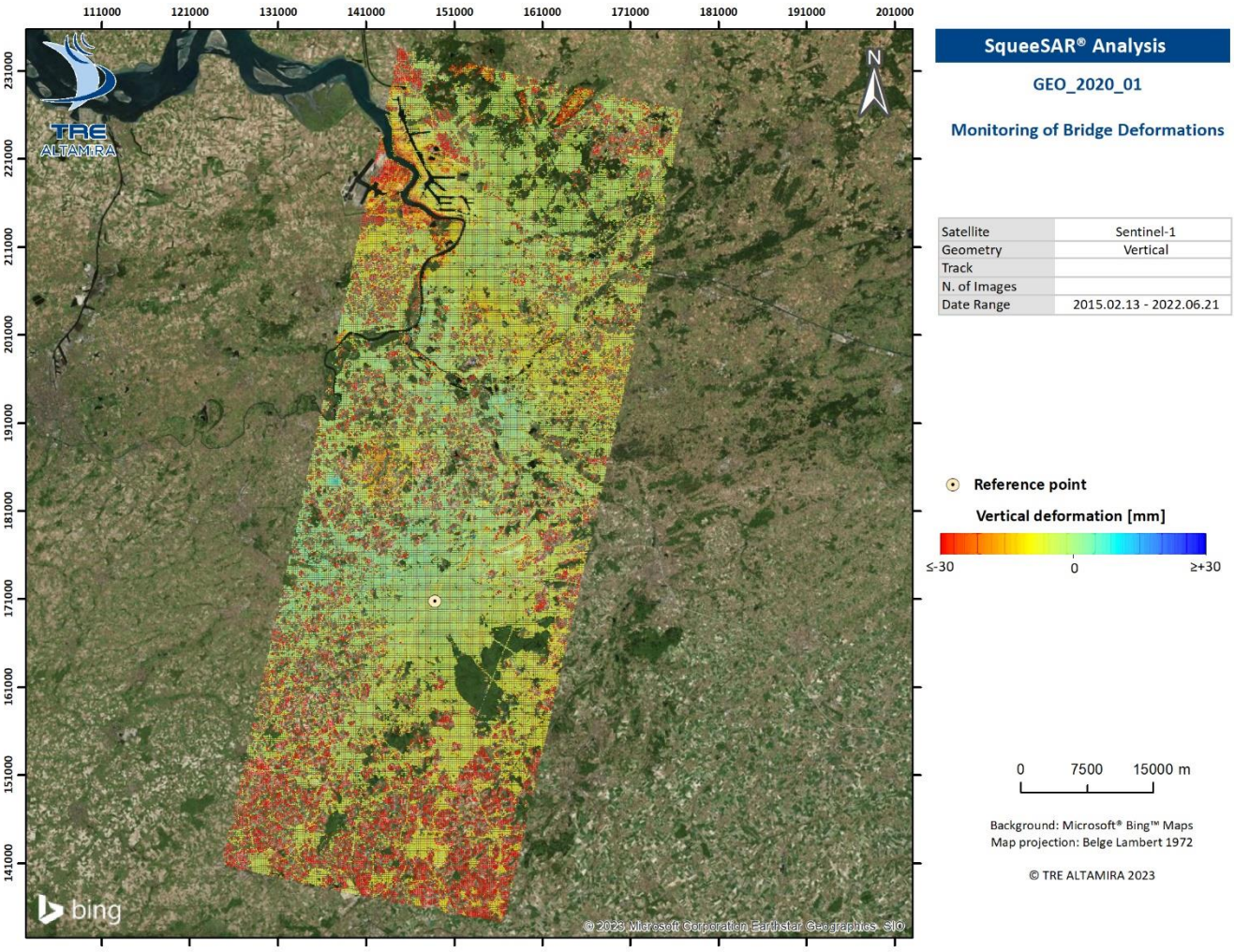

Figure 21: Vertical deformation from the descending and ascending geometries (2D decomposition) of SNT SqueeSAR® analysis.

The horizontal deformation rate in millimetres per year from the SNT descending and ascending archives (2D decomposition) is shown in Figure 22. The deformation rate ranges from -61 mm/yr to 69 mm/yr with a mean value of 1 mm/yr and a standard deviation of ± 6 mm/yr (Figure 22).

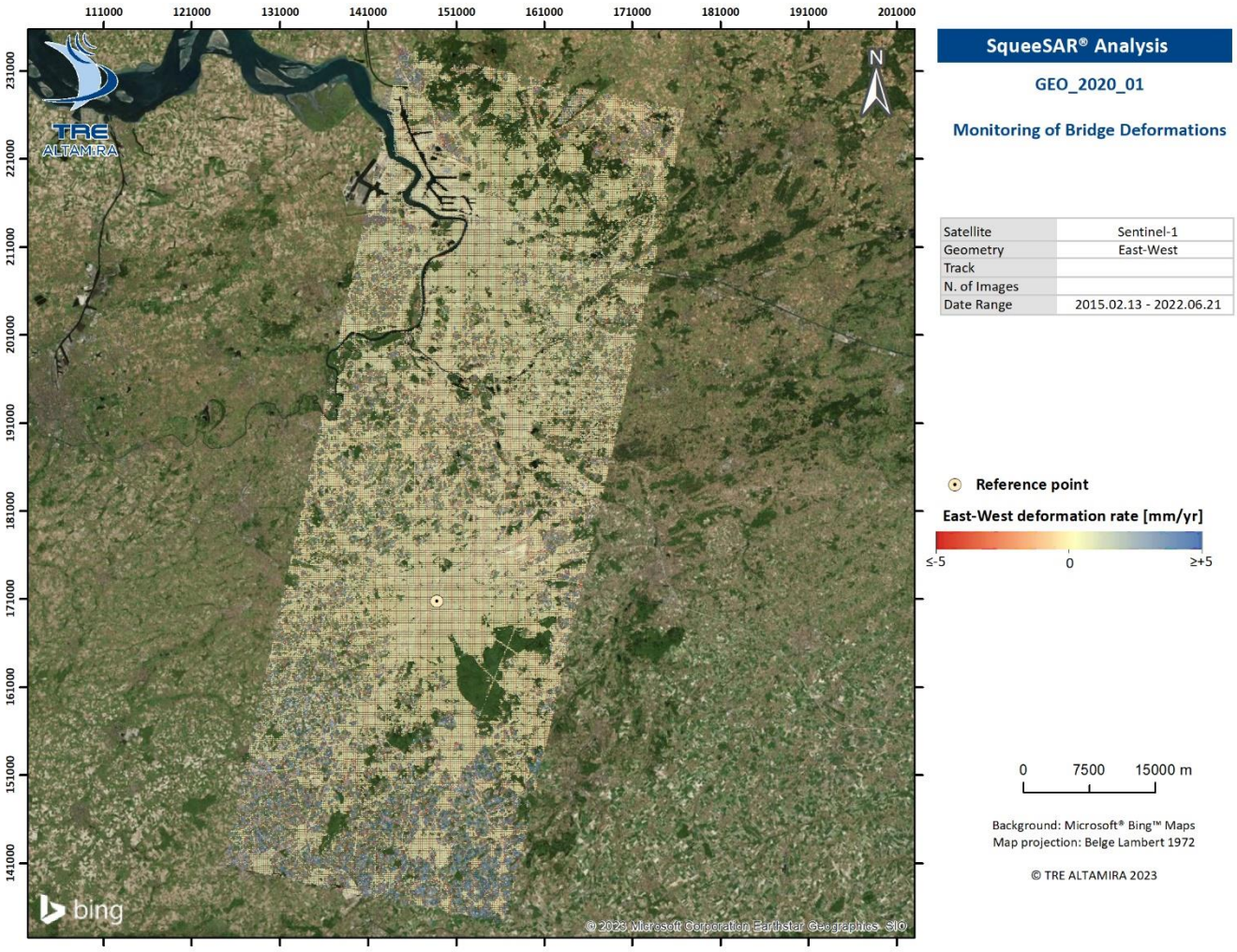

Figure 22: Horizontal deformation rate from the descending and ascending geometries (2D decomposition) of SNT SqueeSAR® analysis.

The horizontal deformation in millimetres from the SNT descending and ascending archives (2D decomposition) is shown in Figure 23. The deformation ranges from -460 mm to 511 mm with a mean value of 8 mm and a standard deviation of ± 41 mm (Figure 23).

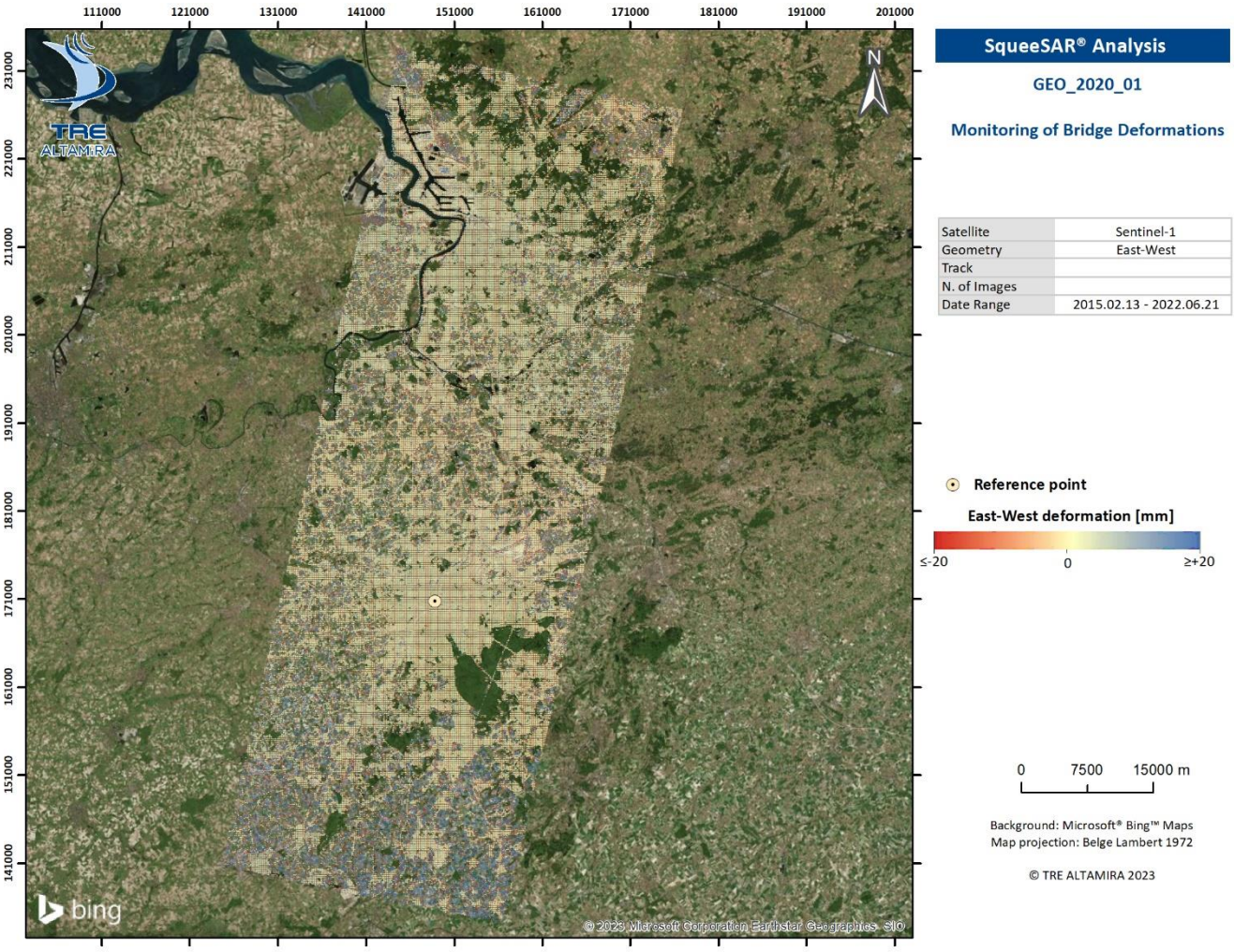

Figure 23: Horizontal deformation from the descending and ascending geometries (2D decomposition) of SNT SqueeSAR® analysis.

The LOS deformation rates measured in millimetres per year from the TSX descending archive are shown in Figure 24. The deformation rate ranges from -63 mm/yr to 28 mm/yr with a mean value of 0 mm/yr and a standard deviation of ± 1 mm/yr (Figure 24).

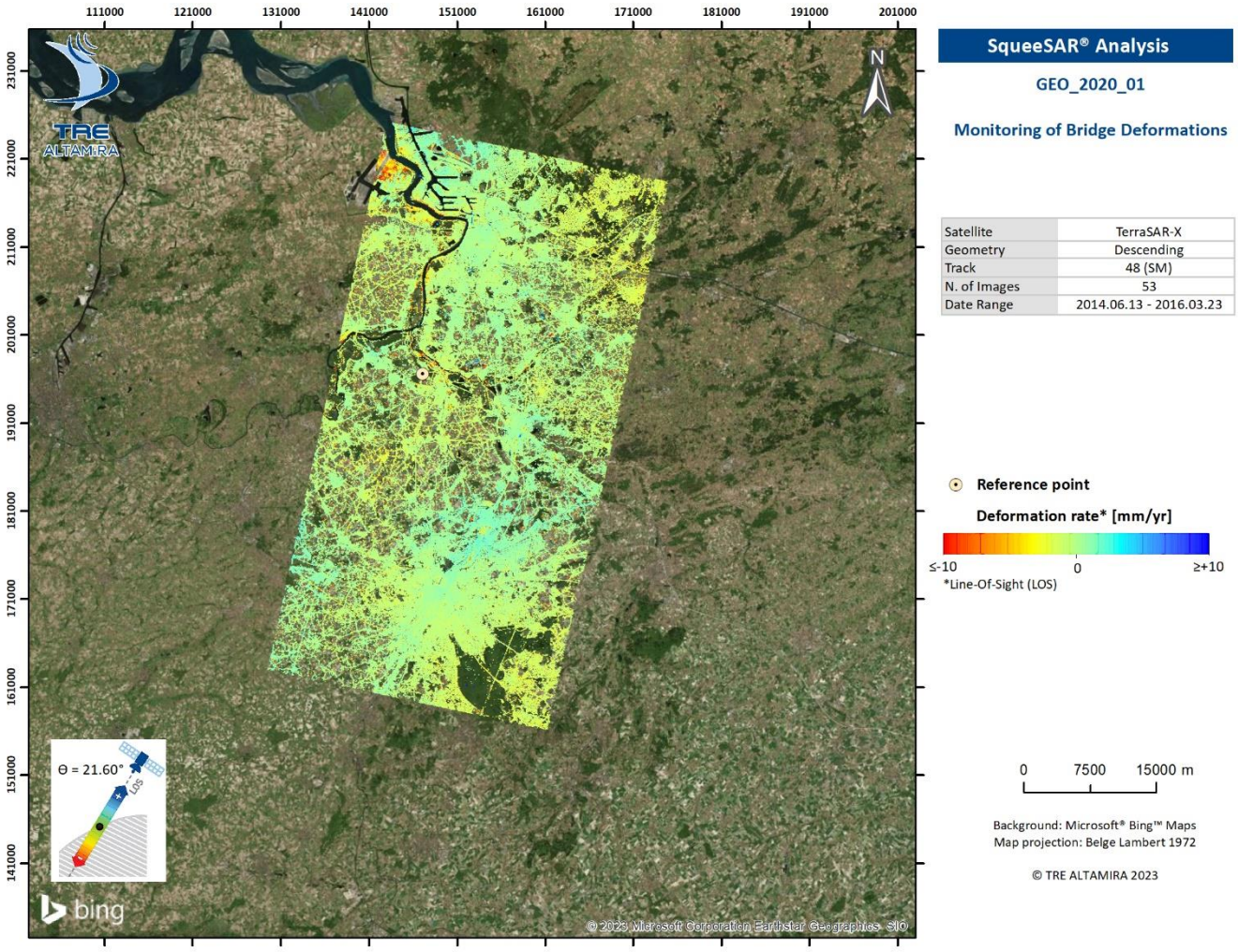

Figure 24: LOS deformation rate from the descending geometry of TSX SqueeSAR® analysis.

The LOS deformation measured in millimetres from the TSX descending archive is shown in Figure 25. The deformation ranges from -113 mm to 45 mm with a mean value of 0 mm and a standard deviation of ± 3 mm (Figure 25).

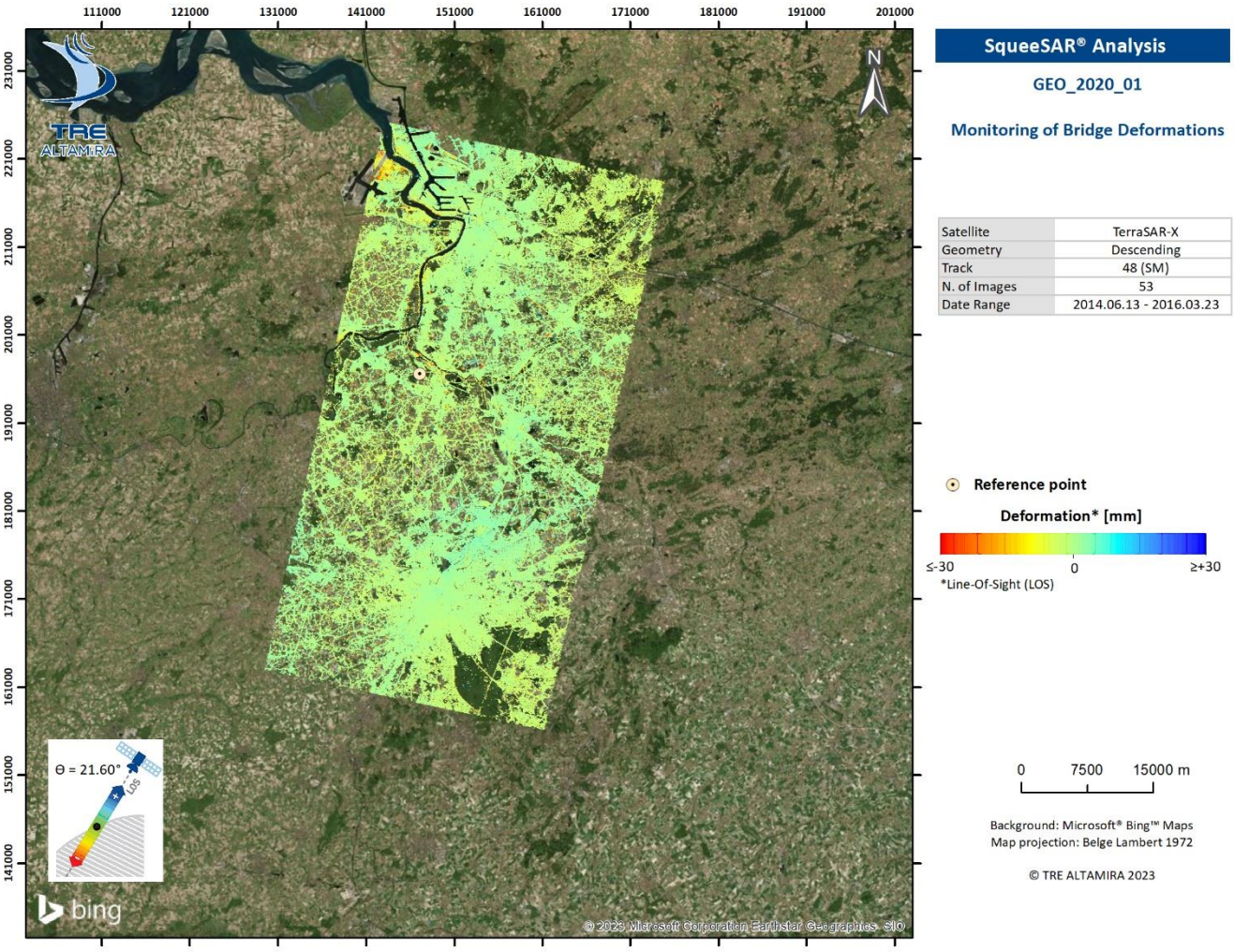

Figure 25: LOS deformation from the descending geometry of TSX SqueeSAR® analysis.

4.4. Seasonal Amplitude maps

The seasonal (annual) amplitude in millimetres from the SNT descending archive is estimated from a sinusoidal adjustment and is shown in Figure 26. The seasonal amplitude reaches a maximum of 14 mm (Figure 26).

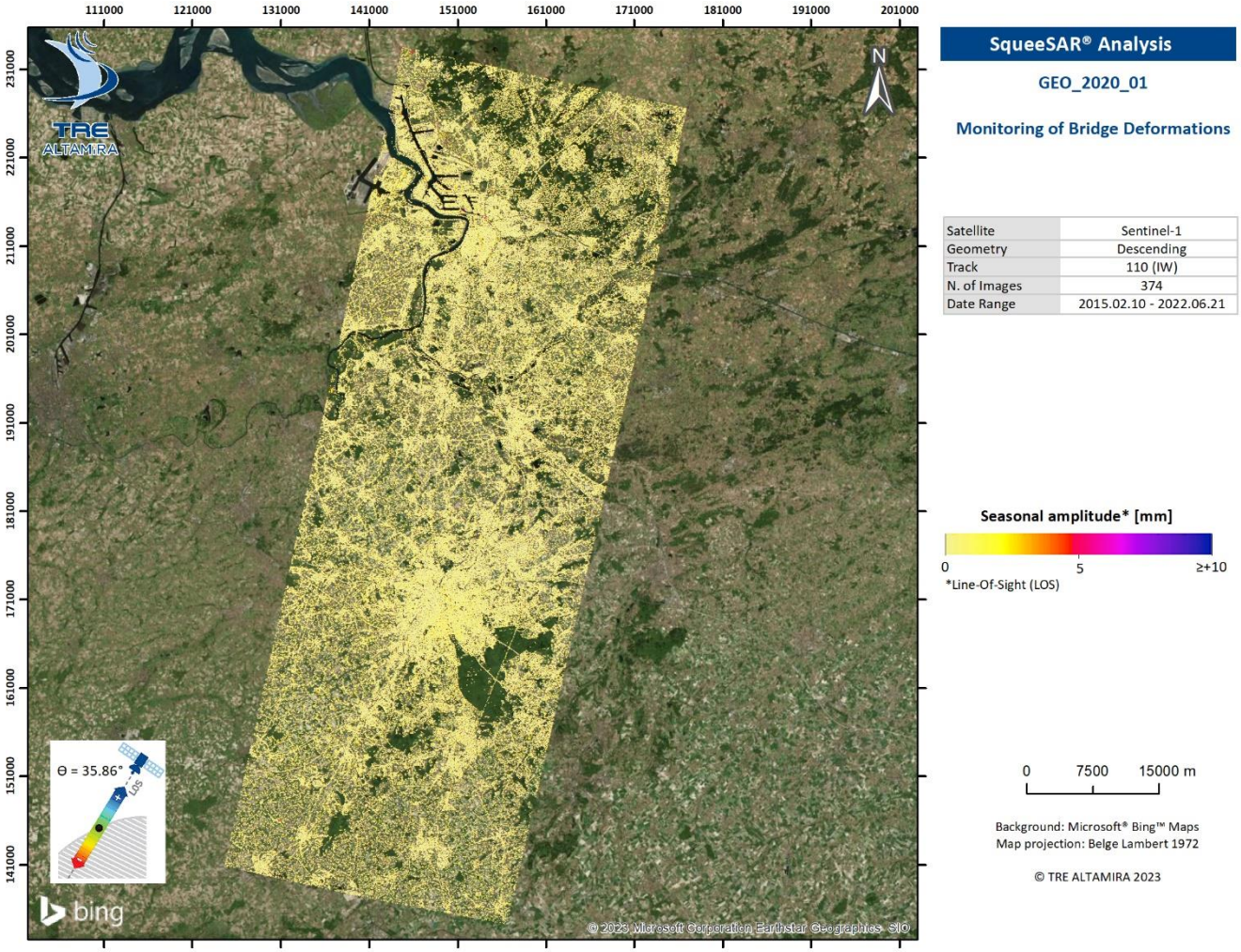

Figure 26: Seasonal (annual) amplitude from the descending geometry of SNT SqueeSAR® analysis.

The seasonal (annual) amplitude in millimetres from the SNT ascending archive is estimated from a sinusoidal adjustment and is shown in Figure 27. The seasonal amplitude reaches a maximum of 20 mm (Figure 27).

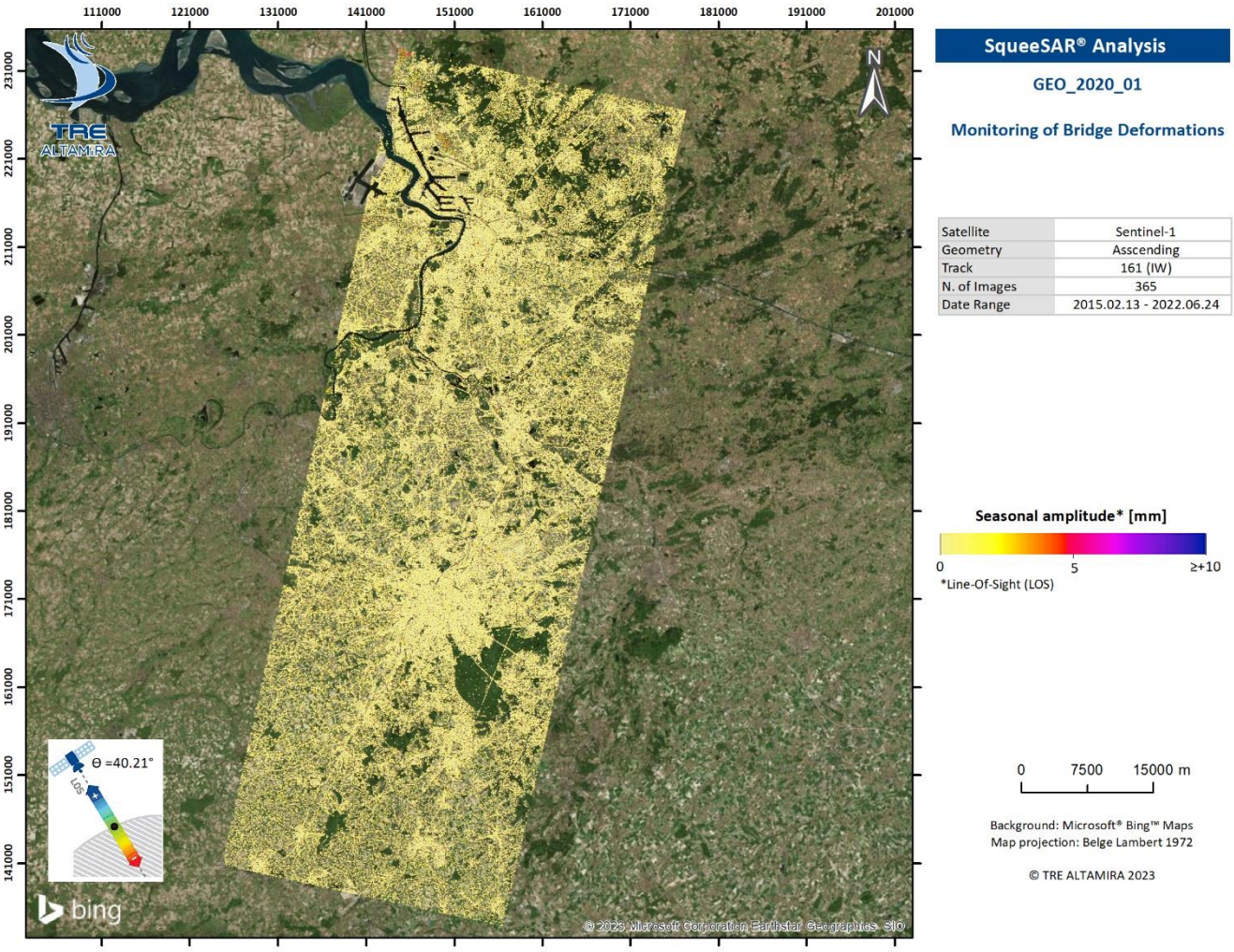

Figure 27: Seasonal (annual) amplitude from the ascending geometry of SNT SqueeSAR® analysis.

The seasonal (annual) amplitude in millimetres from the TSX descending archive is estimated from a sinusoidal adjustment and is shown in Figure 28. The seasonal amplitude reaches a maximum of 14 mm (Figure 28).

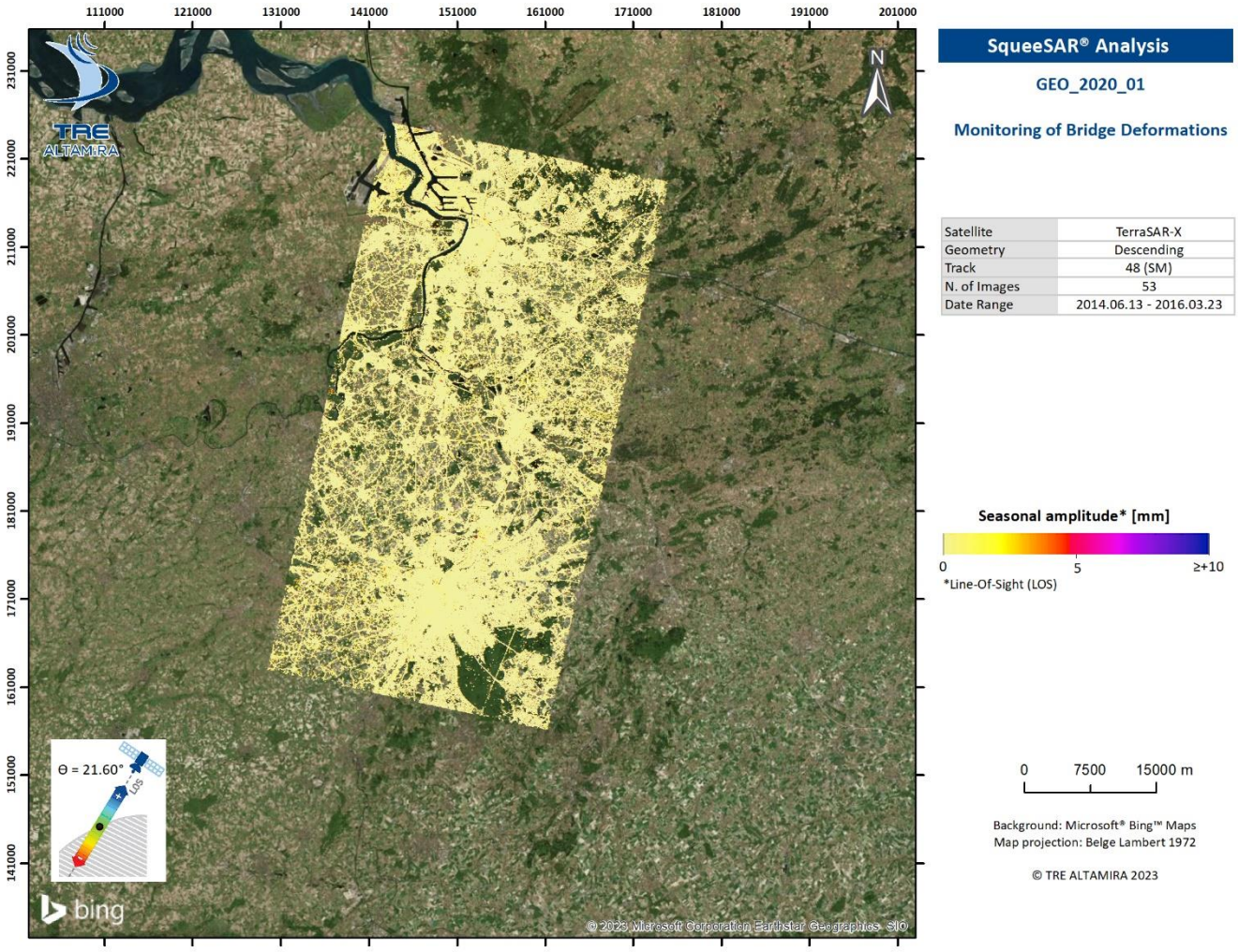

Figure 28: Seasonal (annual) amplitude from the descending geometry of TSX SqueeSAR® analysis.

4.5. Temporal observation

4.5.1. Time series analysis

SqueeSAR® results allow the analysis of each MP's temporal behaviour by displaying their time series. Figure 29 shows an example of the temporal behaviour of 5 MPs over a bridge of the city of Grimbergen (inside the blue circle) from the TSX SqueeSAR® analysis.

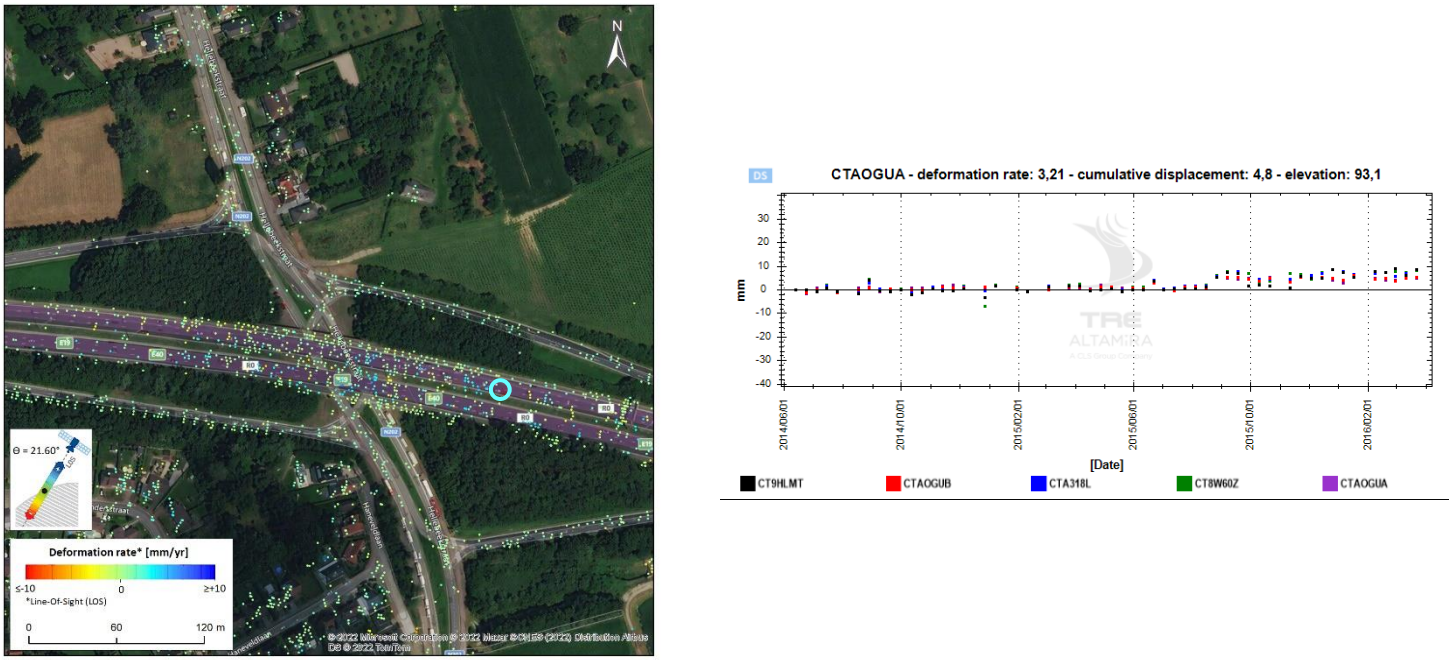

Figure 29: Left: TSX SqueeSAR® deformation rates (mm/yr). Right: Time series of the MPs inside the blue circle.

4.5.2. Deformation profile analysis

SqueeSAR® results allow us to analyse the spatiotemporal behaviour of all the MPs over a single bridge with a deformation profile. Figure 30 shows an example of the spatiotemporal behaviour of all MPs over a bridge in the city of Grimbergen. The deformation profile has a node every 20 m with cells 20 m long and 30 m wide, for example.

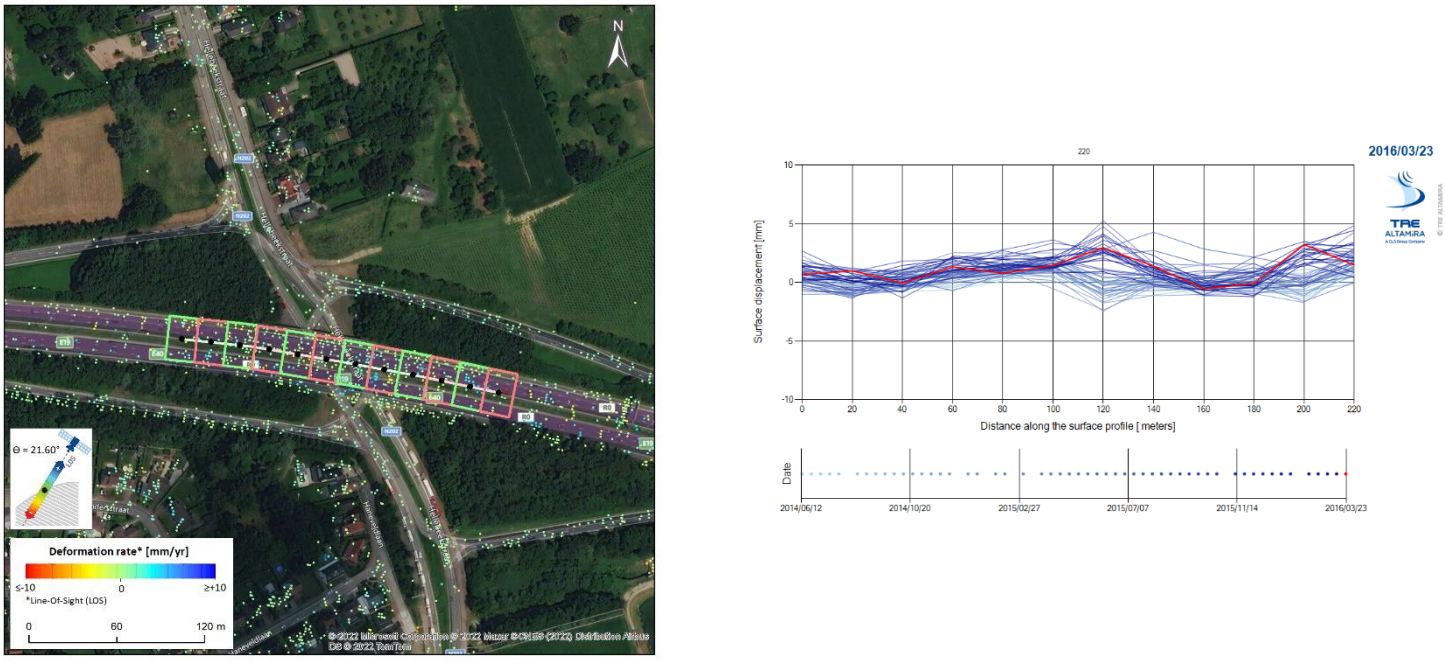

Figure 30: Left: TSX SqueeSAR® deformation rates (mm/yr). Right: Associated deformation profile.

The number of nodes, length, and width of each cell of the deformation profile is adjustable; it can also be carried out on the flight on the TREmaps® web visualiser.

5. Requirements

For this project, which aims to monitor the deformations of the bridges, an essential step in the analysis is represented by using the positions of the bridges during the processing of the SAR images.

Bridges present some challenges for InSAR processing. Indeed, the bridge's metal structure influences the deformation dynamics they undergo. The greater dynamics with respect to the different buildings in the vicinity or the surrounding area create clear discontinuities in the deformation field of the whole analysed area. This leads to possible unwrapping errors (see section 2.5). Accurately identifying the position of the bridges allows for spatially thickening the grid of MPs in the vicinity of these structures, minimising the differential displacement between neighbouring MPs. This way, the possibility of measurement errors on those structures is negligible. This procedure also proves to be fundamental in the case of analysis of large surfaces.

5.1. Maximum availability of results in case of works and in-depth analysis of zone where no InSAR points are available

As previously explained, the MPs included in the SqueeSAR® database present an overall quality larger than the one which ensures meeting the quality standards. Still, some MPs may present a significant loss of quality in one or many parts of the displacement time series. If that is the case, they are identified and excluded from the final result. A methodology based on the MP amplitude value study has been carried out to locate and “save” the temporal period, still presenting a quality displacement.

The amplitude of a SAR image is a measurement of the incident and backscattered energy rate over the illuminated target. Large amplitude values, appearing as brighter pixels, backscatter to the SAR antenna in almost all incident SAR signals. Low amplitude values, appearing as darker pixels, are those whose incident SAR signal is spread over other directions in addition to the incident one, so just a small part of the incident signal is backscattered to the SAR antenna. In that case, the low signal-to-noise ratio leads to a poorer phase quality and a more inaccurate displacement measurement.

The geometry and type of material of the illuminated object drive the amplitude value. Therefore, if the object’s geometry is significantly modified, a change in the amplitude values arises. In the case of significantly decreasing the amplitude (low signal level), a change in the quality of the displacement estimation can be provoked (or the other way around). The idea is to identify both amplitude and quality displacement changes correlated with time.

Firstly, after statistical analysis, the probability of having a significant relative amplitude change is calculated for all the images, so those overpassing a threshold value are detected, identifying the date of the change. Secondly, a similar approach is followed, detecting when a significant change in the displacement variance occurred. If both dates are equal, then that point is identified and saved in a database similar to the SqueeSAR® one, including its displacement variance change and, most importantly, the date(s) from which the displacement time series is reliable. The following fields describe the change parameters:

- INDX_CHNG: Index of the First Change Image on the displacement Time Serie.
- DATE_CHNG: Date of the First Change Image on the displacement Time Serie.
- INDX_CEND: Index of the Second Change Image on the displacement Time Serie.
- DATE_CEND: Date of the Second Change Image on the displacement Time Serie.
- DIFFR_DIS: displacement standard deviation difference (1) of the pre and post-change TS. This magnitude is equal to the difference between the standard deviation of the pre-change displacement Time Series and the standard deviation of the post-change displacement Time Series (DIFFR_DIS = $\sigma_{D\ pre}$ - $\sigma_{D\ post}$). A positive value means improving displacement quality, while a negative value means degrading the displacement quality.

The analysis has been carried out on SqueeSAR® TSX and SNT MPs belonging to the bridge's polygons. No points were identified in the SNT dataset, while few cases of significant changes were identified in the TSX dataset. In Figure 31, Figure 32 and Figure 33, some examples of the detected changes are illustrated. Among them, in the upper part, the temporal displacement series is plotted; in the lower part, the plotted magnitude is the temporal amplitude series. In all three cases, it can be noticed that a significant rise in the amplitude took place. At the same time, after the date of the change, the displacement samples improved their quality, passing from a noisy regime to a less dispersive one. Consequently, the reliable period of displacement is considered from that change date.

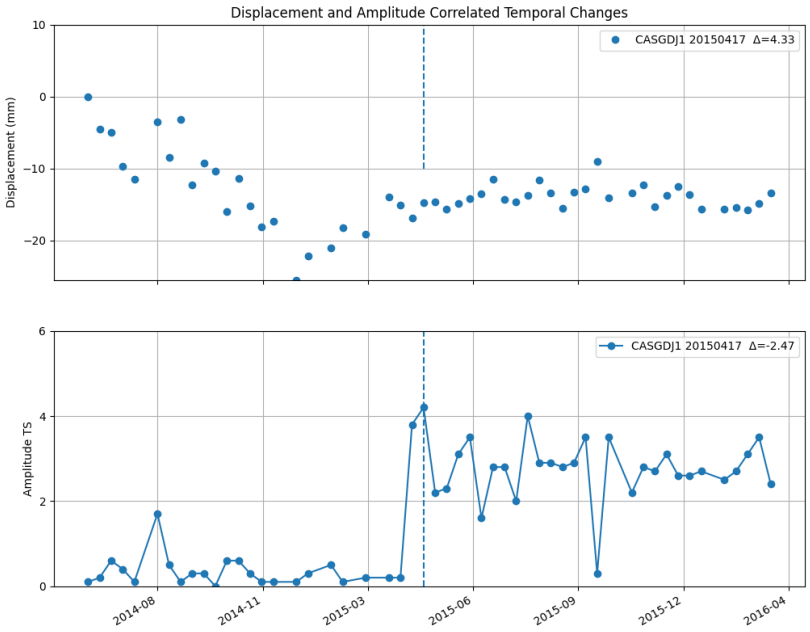

Figure 31: Upper: TSX CASGDJ1 point displacement Time Serie, Δ represents the displacement standard deviation change difference. Lower: TSX CASGDJ1 amplitude Time Serie, Δ represents the amplitude change difference. A permanent significant amplitude change has been identified from 20150417 on.

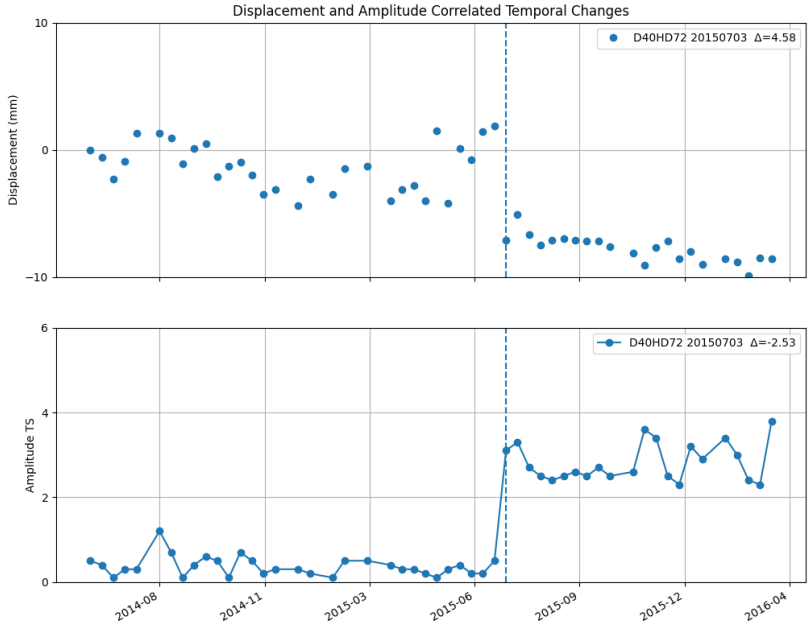

Figure 32: Upper: TSX D40HD72 point displacement Time Serie, Δ represents the displacement standard deviation change difference. Lower: TSX D40HD72 amplitude Time Serie, Δ represents the amplitude change difference. A permanent significant amplitude change has been identified from 20150703 on.

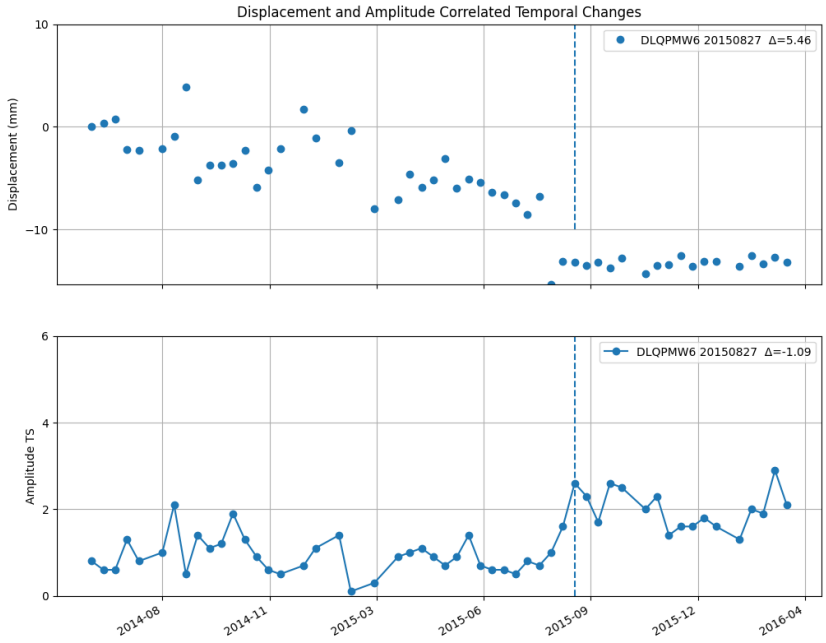

Figure 33: Upper: TSX DLQPMW6 point displacement Time Serie, Δ represents the displacement standard deviation change difference. Lower: TSX DLQPMW6 amplitude Time Serie, Δ represents the amplitude change difference. A permanent significant amplitude change has been identified from 20150827 on.

5.2. Surroundings

The results of the InSAR analysis in the bridge's surroundings are available. It is clear which MPs are located on the bridge and which are not located on the bridge, and for which MP this is uncertain. This classification will help to differentiate which part of the deformation is on the bridge and which is located in the bridge's surroundings.

TRE Altamira has developed a methodology using the a priori information of the bridge boundaries and the estimated individual parameters of absolute HEIGHT and DEM correction from the SqueeSAR® analysis for each MP. Based on the latter, **the overall statistics of the average height and the standard deviation of each detailed part from each bridge are estimated**. A new field, "SURR_CLASS", is added to a dedicated shapefile containing the MPs within a buffer of 20 m inside and around each bridge. Table 9 presents explanations related to each value of the SURR_CLASS field.

Surrounding Classification "SURR_CLASS"	Class Definition
0	MPs that are external to the bridge, or MPs that are on the ground or with an inconclusive height in comparison with the average height of the bridge
1	MPs that there is uncertainty whether they are in the bridge deck or in the ground or other external structures that are within the bridge boundary or very close surroundings (6 meters as maximum)
2	MPs that are on the bridge deck or structures with similar height or MPs that are within the bridge boundary or very close surroundings and have similar height to the average height of the bridge

Table 9: Satellite acquisition parameters and image acquisition information.

Geolocation inaccuracies and height corrections may cause minimum misalignments between the bridge edges and some external MPs with similar parameters to the bridge MPs. Thus, external MPs within the limits of the bridge have been considered and classified. The distance considering the external MPs has been set up to 6 meters, and the criteria have been linked to the same statistics of the reliable MPs on the bridge.

Figure 34 presents an example of the MP's heights around the Viaduct von Vilvoorde and the corresponding classification.

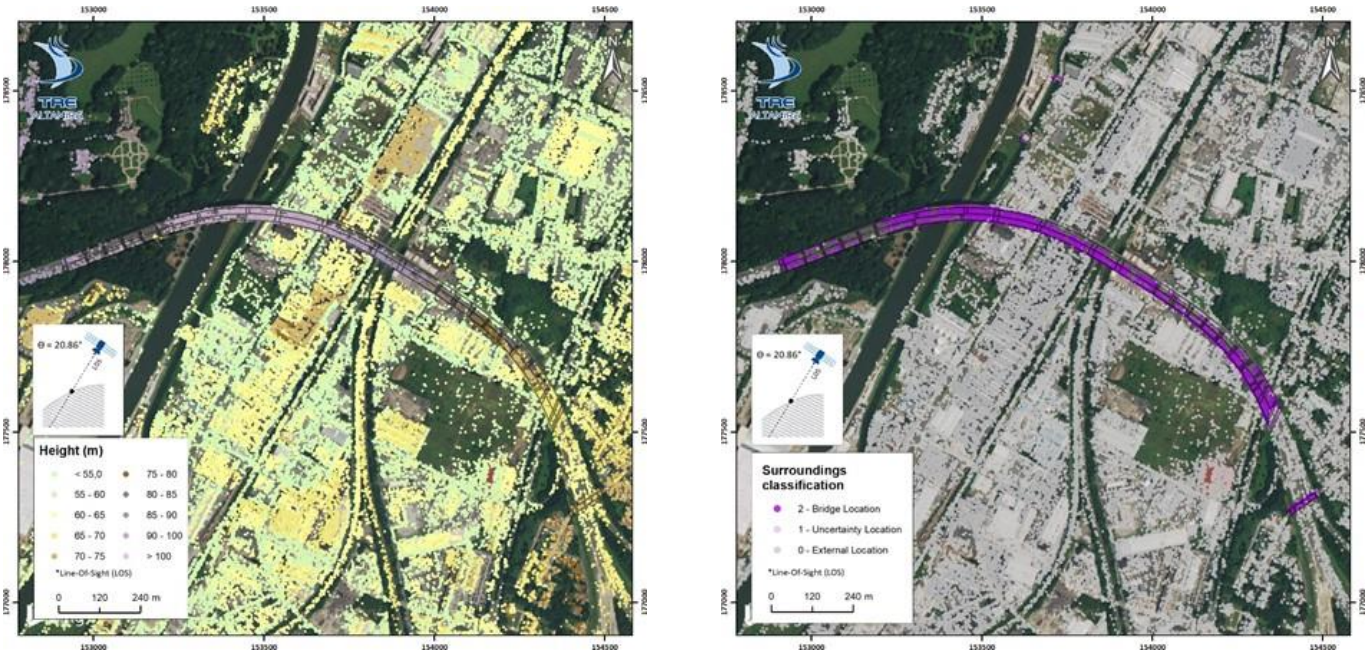

Figure 34: Left: Height of the MP in the vicinity of the Viaduct van Vilvoorde. Right: Classification of the MP in the vicinity of the Viaduct von Vilvoorde.

5.3. Automation of longitudinal profiles

A semi-automated approach has been devised to produce the profile deformation plots for each bridge in the database supplied by the client for the three LOS solutions processed on this project. The client specified that in addition to the whole extent of the bridges, each profile should cover 20 metres at each end of the structure (Figure 35).

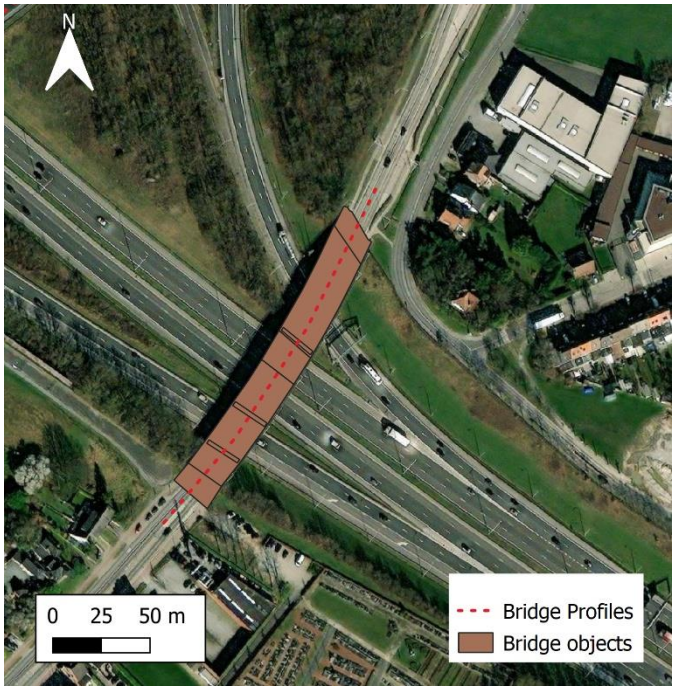

Figure 35: Example of the profile length compared to a bridge.

Each solution requires a different approach to the polygons used to average the deformation values of the MPs present over the footprint of the structures. For the high-resolution solution, a 10 m square polygon has been used for all the structures, given the radar images' pixel size and square shape.

The mid-resolution processing requires a different approach since the pixel size is asymmetrical (5 x 20 m). This factor makes it necessary to assess the orientation of each structure relative to the satellite orbit path for each geometry, as the MP coverage can vary significantly from a structure perpendicular to the orbit path to a parallel one. The orientation of the long edge of each structure has been calculated using GIS geoprocessing to determine the cell length for each of them. All the SNT polygons are defined between a bracket of 10 m to 40 m in length, which is automatically adjusted based on the orientation of each structure for both ascending and descending geometries.

Figure 36 shows how the profile cells change depending on the orientation of a series of mock-up bridges compared to the satellite trajectory. The polygon width used is the same as with the high-resolution, given the average of the structures, with a value of 10m.

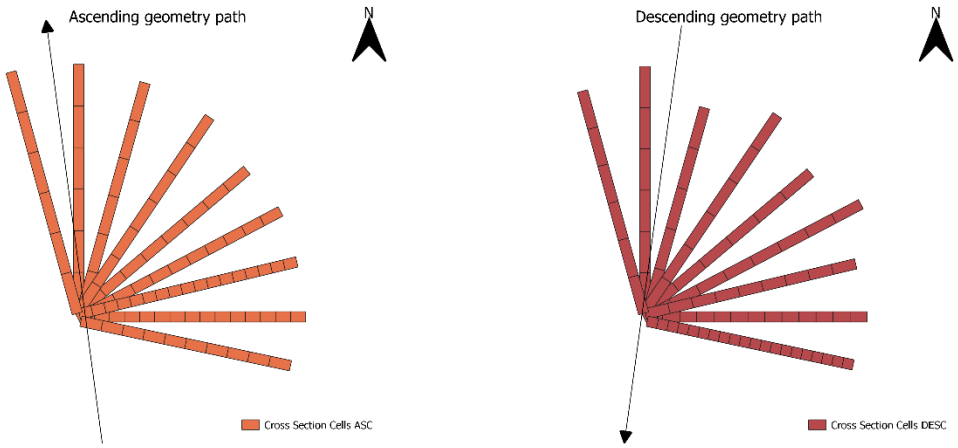

Figure 36: The left image illustrates the length of the profile average cells based on the structure's orientation versus the ascending orbit path for Sentinel-1 imagery, whilst the right image showcases the lengths used for the descending geometry.

The three sets of profile cells are then used to obtain the average displacement values for each acquisition of each processing. The output of such calculation is then used to plot the profile for each solution. Cells containing no measurement points are not displayed on the plots.

Another requirement was to produce bridge sketches to compare the deformation plots with the relevant parts of each structure analysed. This has been achieved using the profile lines used as the starting point for the profile plots and the bridge object database supplied by the client. The profile lines are clipped to each intersecting element of each bridge using batch GIS geoprocessing and then merged into a separate database linking each profile with the bridge elements and their geospatial properties (Figure 37).

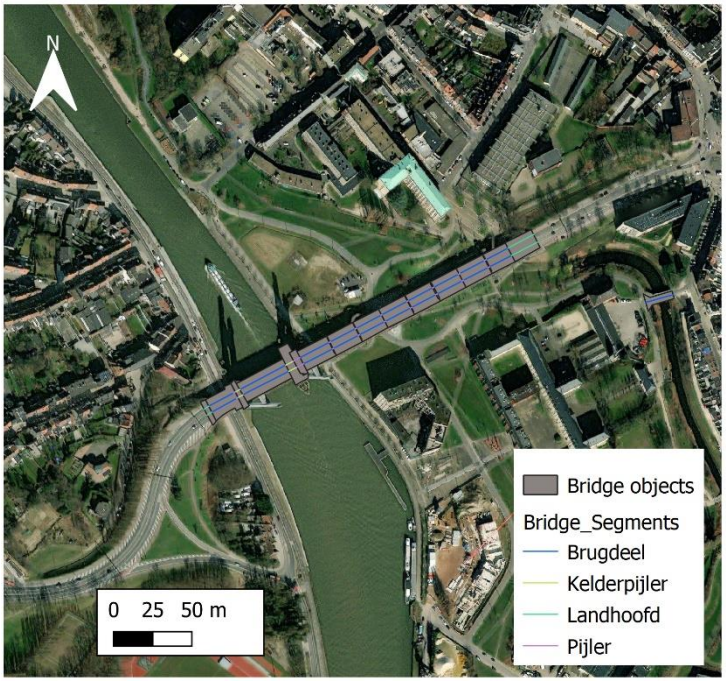

Figure 37: Example of the different bridge parts intersection of the profile lines used for the profile plots compared to the bridge object database supplied by the client.

All the aforementioned datasets are combined in an automated process that blends the deformation profiles for each solution, a graphical representation of the relevant temporal coverage processed and the bridge or structure sketch.

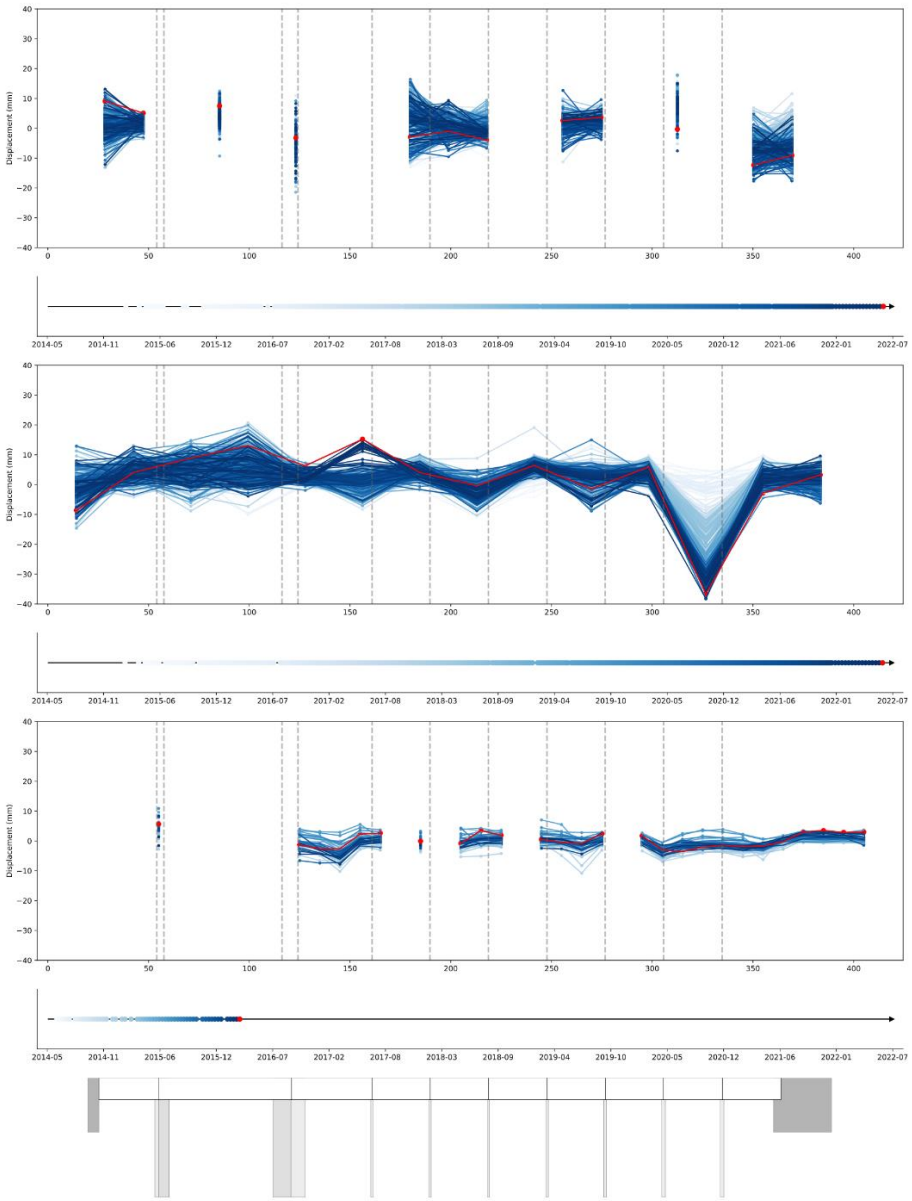

Figure 38. Example of the multi-chart automated profile plot with a bridge sketch and the location of each of the pillars visible on the different deformation profiles.

5.4. Detection of sudden changes in displacement

The SqueeSAR® algorithm is not forced to use a linear model for the displacement estimation, and non-linear or seasonal components (like thermal ones) are managed, preserving MPs with such

behaviour for further analyses. Trend Variation detection can act as an alert system by flagging any time series exhibiting abnormal motion or trend changes.

The Trend Variation (TV) analysis is applied to SqueeSAR® results to support the identification of points with recent changes in the displacement trend (i.e., acceleration, deceleration, or a stepwise movement).

The algorithm is sensitive to rate variations larger than **5 mm/yr** and stepwise displacement (i.e., single jump in the time series) greater than **5 mm**. However, variations are only highlighted when they are greater than the precision parameters (measurement error STD_DEF bar and deformation rate standard deviation V_STDEV) of the measurements (see details below) and are persistent for at least 3 to 4 consecutive images. The parameters used for this study are listed below:

- Change in rate (ΔV) = 5 mm/yr
- Stepwise displacement (Δstep) = 5 mm
- Period of observation (Δt) = 60 days

Figure 39 shows examples of times series that would be highlighted for either a change in displacement trend or an offset in motion.

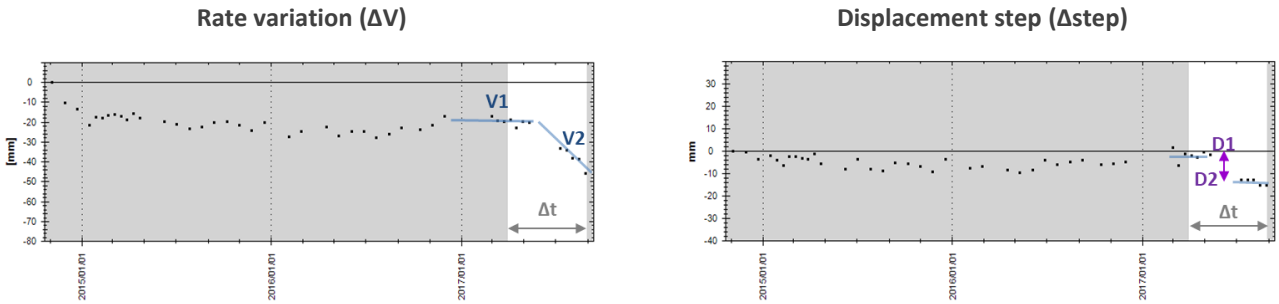

Figure 39: Examples of time series with a recent rate variation or displacement step.

Once a TV has been identified, the output database provides the following:

- Date of when the change in trend occurs (WHEN): it corresponds to the date of the image acquisition when the change in trend is first identified (i.e., not the date when the TV starts to highlight the point).
- Displacement rate before the trend change (V1): it corresponds to the average displacement rate before the change in trend (i.e., linear regression of the time series before the change date).

- Displacement rate after the trend change (V2): it corresponds to the average displacement rate after the change in trend is identified (i.e., linear regression of the time series after the change date).
- Rate variation (DVEL): it describes the difference in the rate before (V1) to and after (V2) the trend change. Note that this value is not the simple difference between (V2) and (V1) but also takes into account the accuracy of the measurements (i.e., only DVEL values that are greater than the standard deviation values of (V1) and (V2) are used for the calculation). Positive DVEL values indicate acceleration, and negative values indicate deceleration.
- Displacement step (DSTEP) quantifies the displacement change between 2 acquisitions (i.e., step in the time series) before and after the stepwise movement. Only DSTEP values greater than the error bars, calculated for both the period before and after the change, are highlighted in the TV analysis and reported in the DSTEP field.

Figure 40 shows the spatial distribution of the MPs whose time series are subject to trend variations regarding the mentioned parameters for the SNT descending geometry.

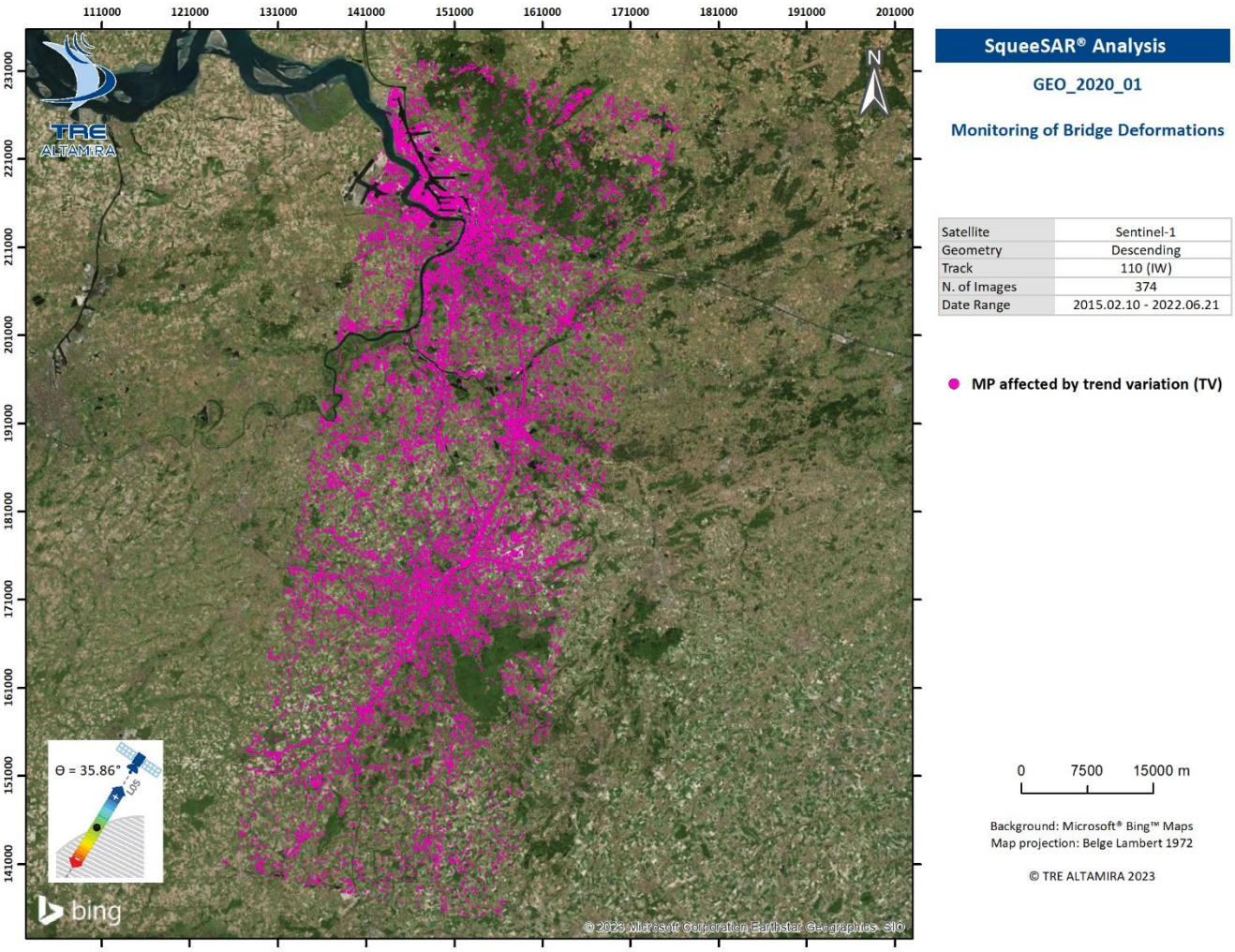

Figure 40: Trend Variation analysis from the descending geometry of SNT SqueeSAR® analysis.

Figure 41 shows the spatial distribution of the MPs whose time series are subject to trend variations regarding the parameters mentioned in the SNT ascending geometry.

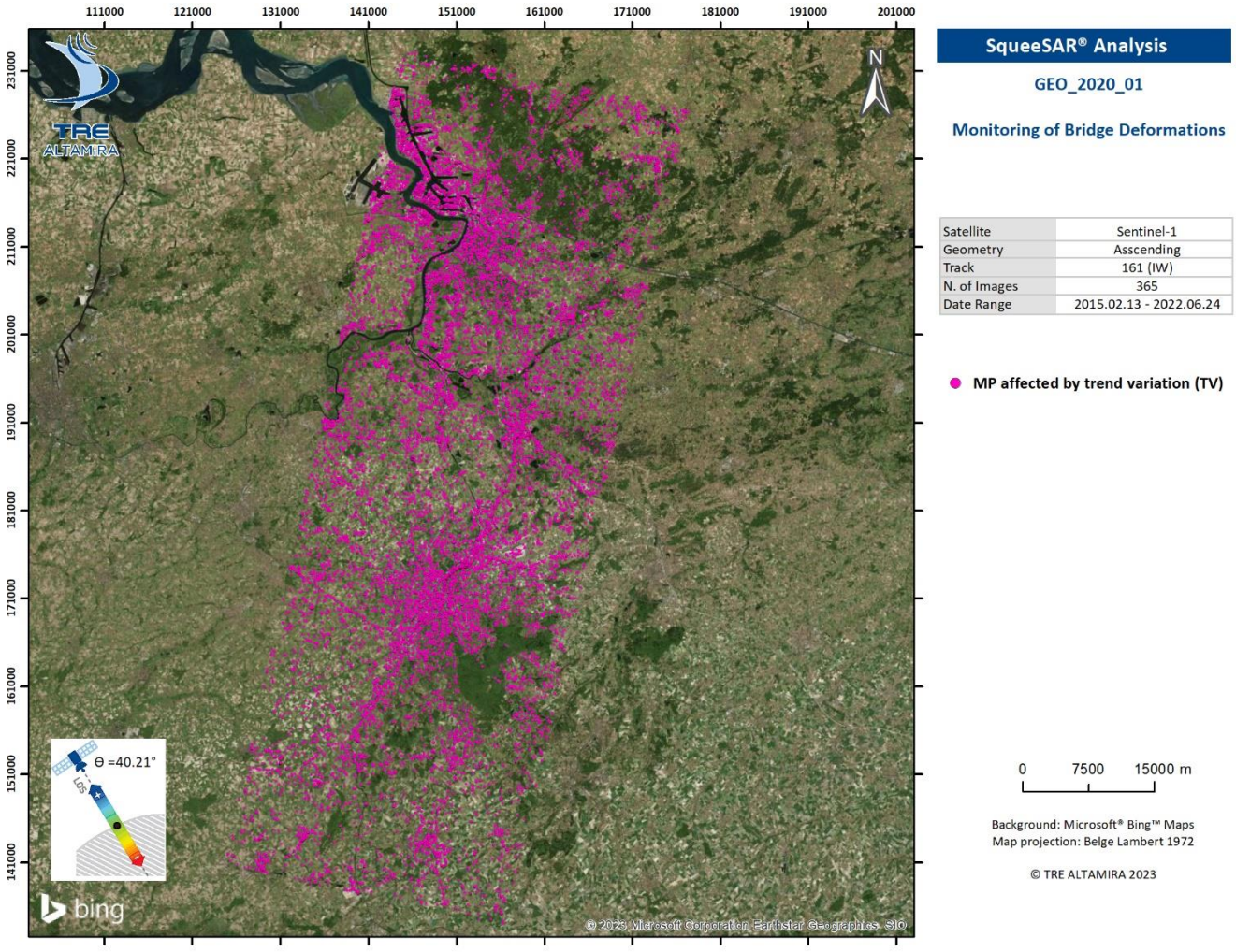

Figure 41: Trend Variation analysis from the ascending geometry of SNT SqueeSAR® analysis.

Figure 42 shows the spatial distribution of the MPs whose time series are subject to trend variations regarding the mentioned parameters for the vertical component of the 2D decomposition (from SNT descending and ascending geometries).

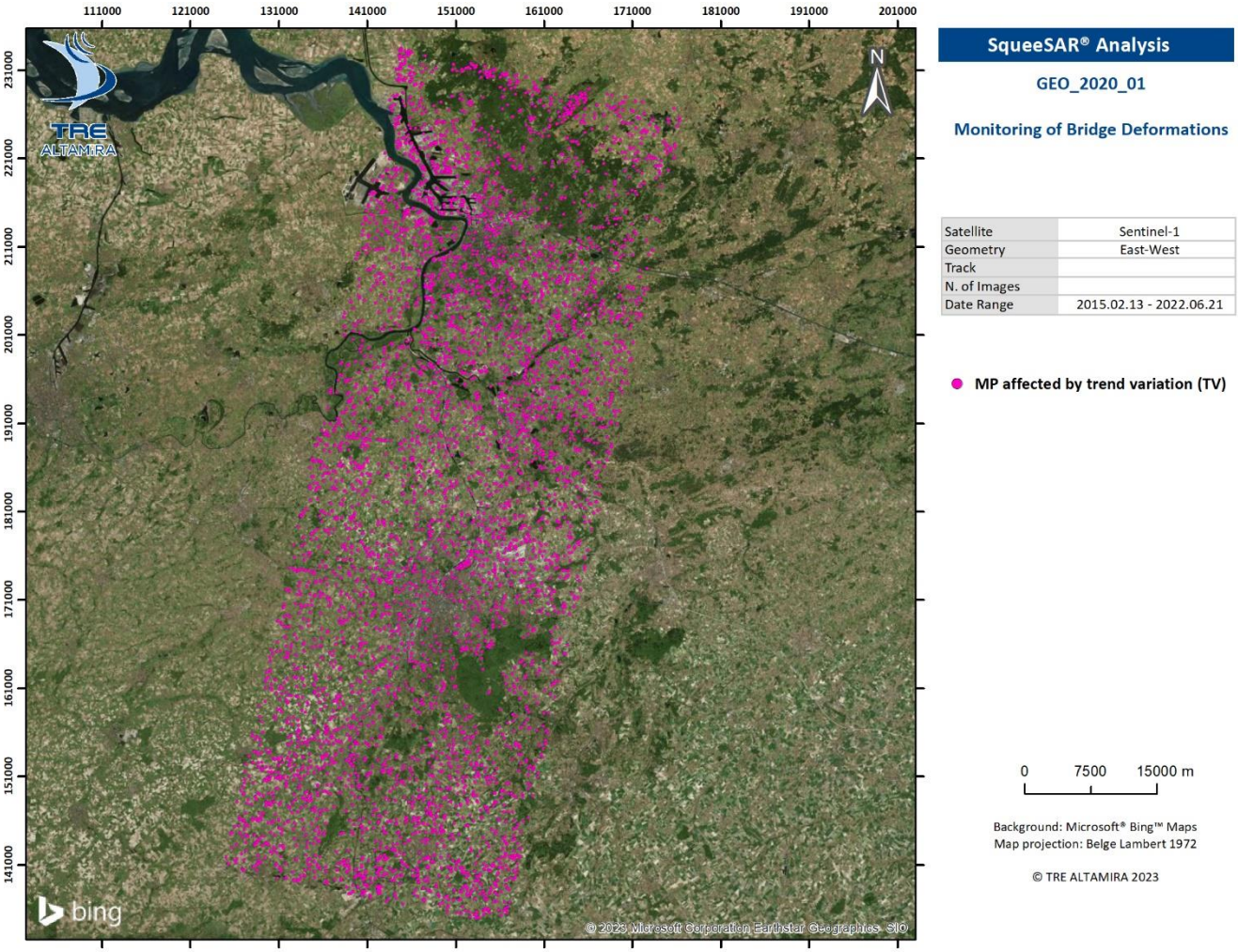

Figure 42: Trend Variation analysis from the vertical component of the 2D decomposition of SNT SqueeSAR® analysis.

Figure 43 shows the spatial distribution of the MPs whose time series are subject to trend variations regarding the mentioned parameters for the horizontal component of the 2D decomposition (from SNT descending and ascending geometries).

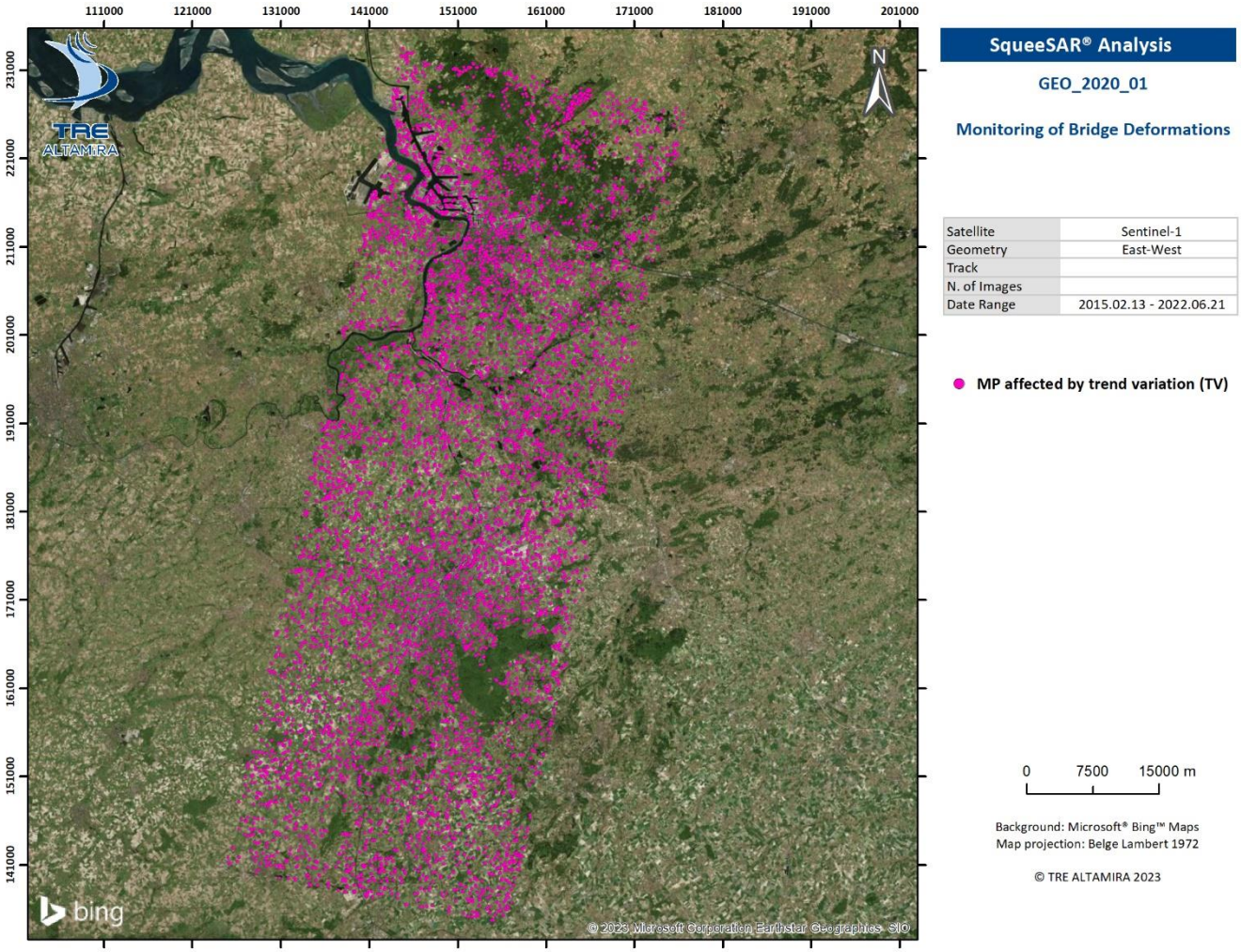

Figure 43: Trend Variation analysis from the horizontal component of the 2D decomposition of SNT SqueeSAR® analysis.

Figure 41 shows the MPs' spatial distribution, whose time series are subject to trend variations regarding the parameters mentioned for the TSX descending geometry.

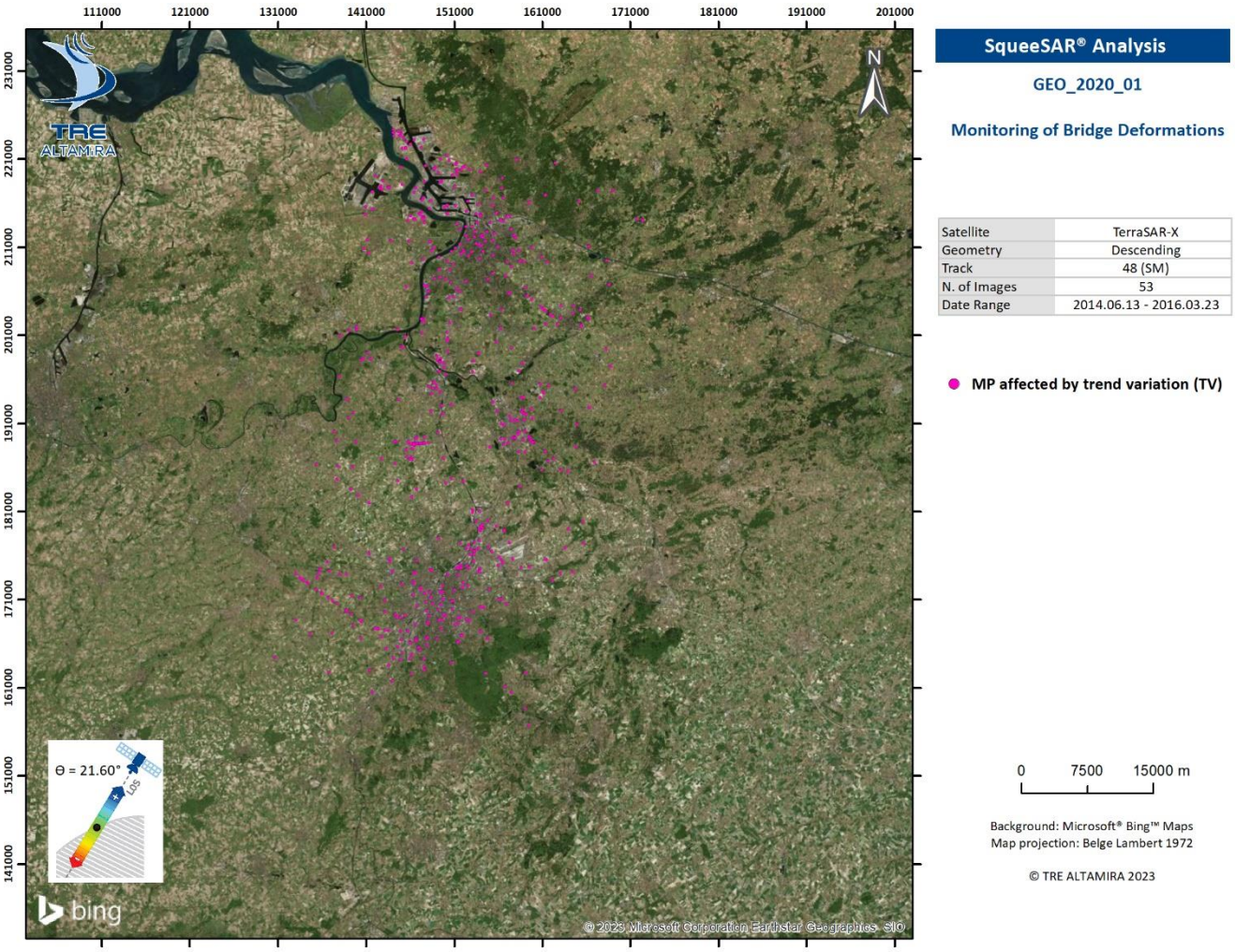

Figure 44: Trend Variation analysis from descending geometry of TSX SqueeSAR® analysis.

The analysis of the time series shows the results from the TSX SqueeSAR® analysis are less subject having MP highlighted by the Trend Variation analysis:

- 692 MPs for TSX in descending geometry for a total of 21 433 890 MPs
- 19 670 MPs for SNT in descending geometry of 8 316 536 MPs
- 19 529 MPs for SNT in ascending geometry of 9 614 837 MPs

Figure 45 presents an example of velocity variation on the left and a stepwise movement on the right.

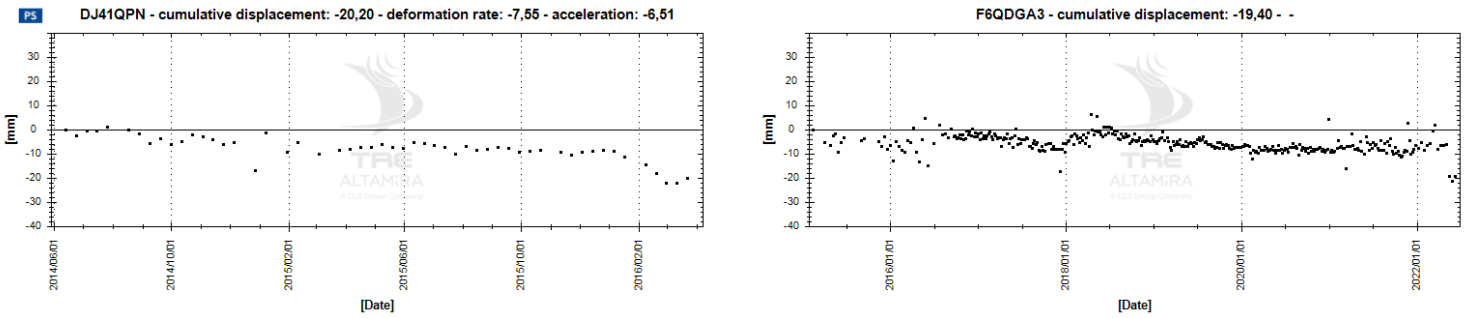

Figure 45: Left: example of a trend variation for the TSX SqueeSAR® analysis in descending geometry. Right: example of a stepwise movement for the SNT SqueeSAR® analysis in ascending geometry.

5.5. Temperature variations

It is fair to consider that seasonal displacement patterns over the MPs in the bridges are temperature driven. Therefore, two main reasons exist to estimate the corresponding thermal motion component. The first is to check whether the thermal response is under the expected behaviour. The second is compensating that component from the total motion to detect other significant motion patterns.

To perform such an estimation, the carried-out solution implies using local temperature. The temperatures corresponding to the dates of all the SAR acquisitions are obtained. To that matter, the https://opendata.meteo.be/ data has been used, particularly the 1-hour temperature database. Since the first available temperature data corresponds to 2017-11-17, the data available on https://www.wunderground.com/ was used to obtain the temperature corresponding to the previous dates.

Once the temperature values are obtained, a polynomial model plus a linear displacement depending on that temperature (therefore, whose resultant value will be the “thermal dilation constant”) will be fitted to the displacement for each MP belonging to the bridge’s surface. The thermal coefficient (mm/Celsius degree) is obtained from this analysis for each MP.

However, the employed temperature could be inaccurate, so a correction of it is performed. Firstly, those points presenting a significant thermal constant value are selected. Then, taking the polynomial model displacement and the thermal coefficient for each of them, the temperature which minimises the residual (displacement minus polynomial and thermal component) quadratic error is calculated for each image date employing all selected points. Being that temperature is the correction factor, the "true" temperature (the initial one plus this correction) is again used to perform again the displacement model adjustment (described in the precedent paragraph), retrieving the thermal component, which is subtracted from the displacement. The thermal constant is expressed in mm/Celsius degrees, and the thermal compensated motion is generated as a result.

In Figure 46, Figure 47 and Figure 48, the employed temperatures are depicted for the TSX dataset, the SNT ascending and the SNT descending, respectively.

In Figure 49, Figure 50 and Figure 51, an example of the thermal compensation for a point in the TSX dataset, the SNT ascending and the SNT descending are plotted, respectively. In them, the upper part represents the original displacement (in black) and the thermal model, i.e., the calculated thermal constant obtained as explained multiplied by the corresponding image temperature. In the lower part of them, the residual, equivalent to subtracting the thermal displacement model from the total displacement, is shown.

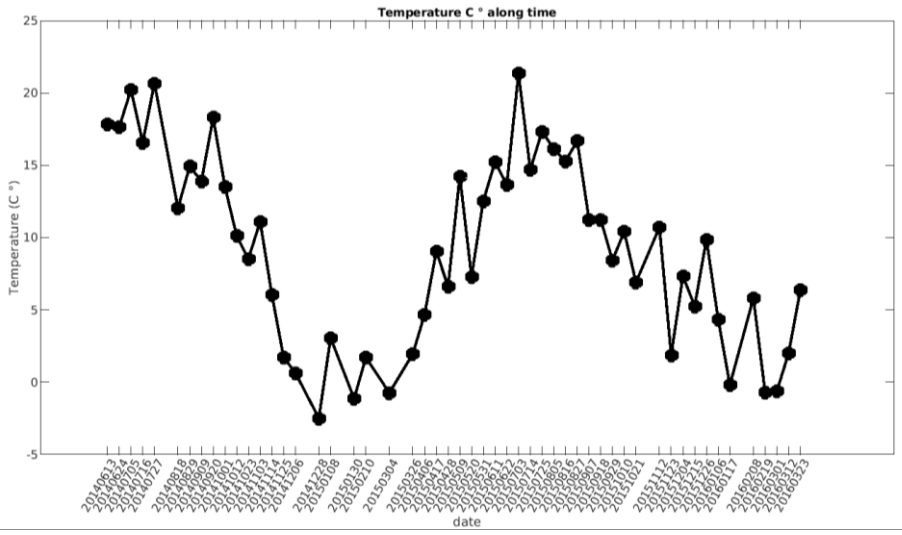

Figure 46: Temperature corresponding to the TSX dataset.

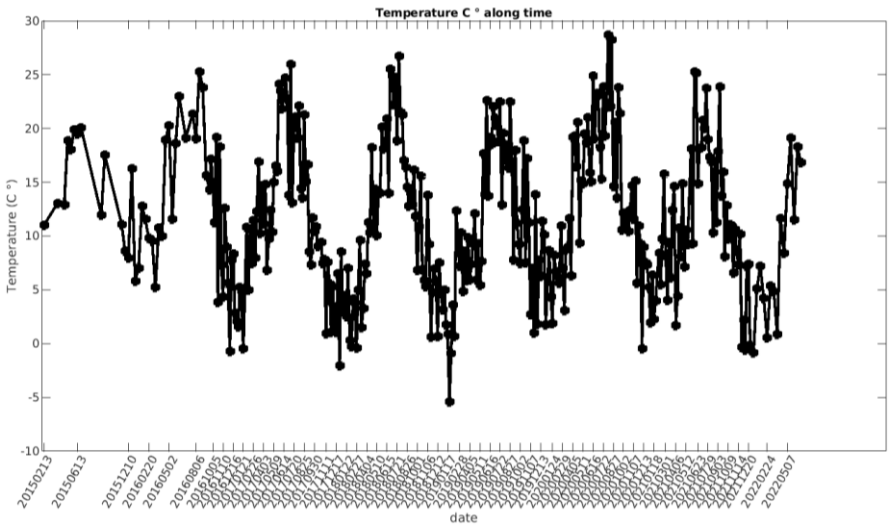

Figure 47: Temperature corresponding to the SNT ascending dataset.

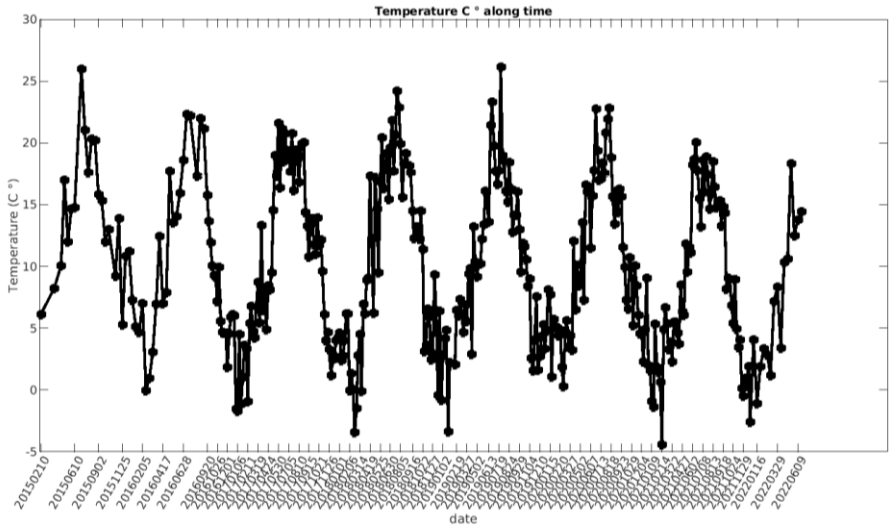

Figure 48: Temperature corresponding to the SNT descending dataset.

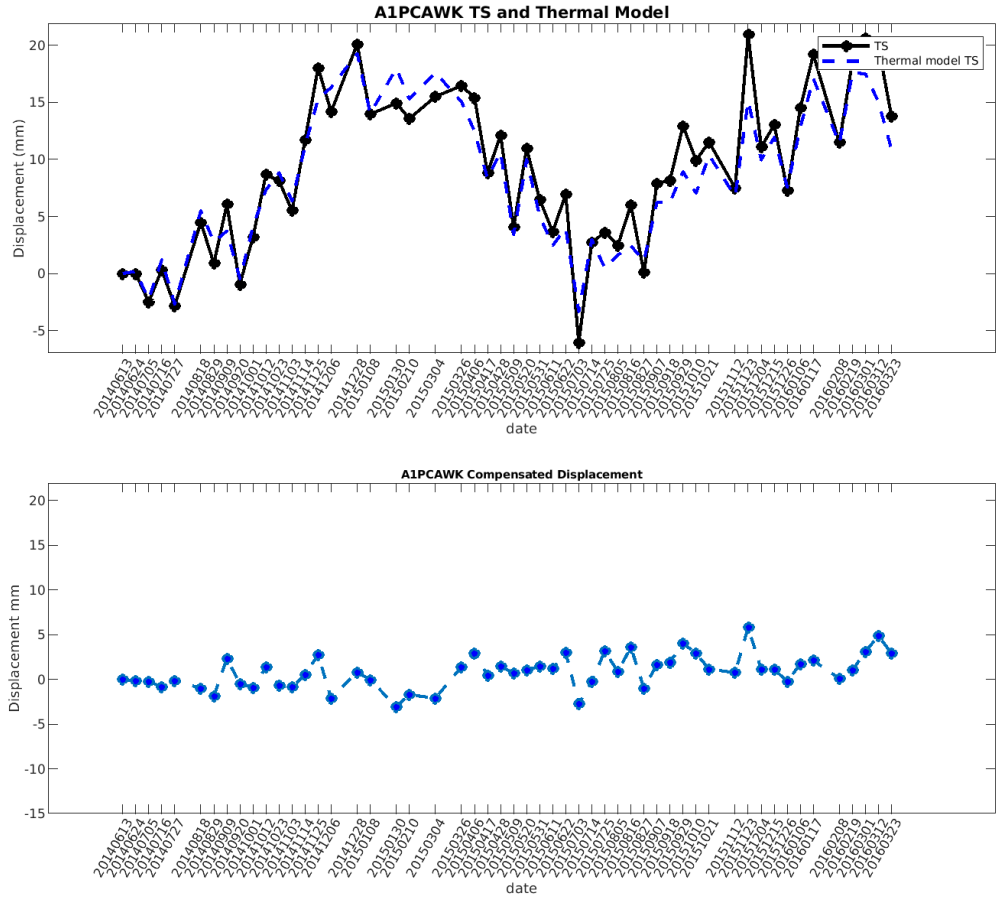

Figure 49: TSX A1PCAWK point. Upper: Displacement Time Series in black and its corresponding thermal displacement model in dashed blue. Lower: thermal model compensated displacement Time Series.

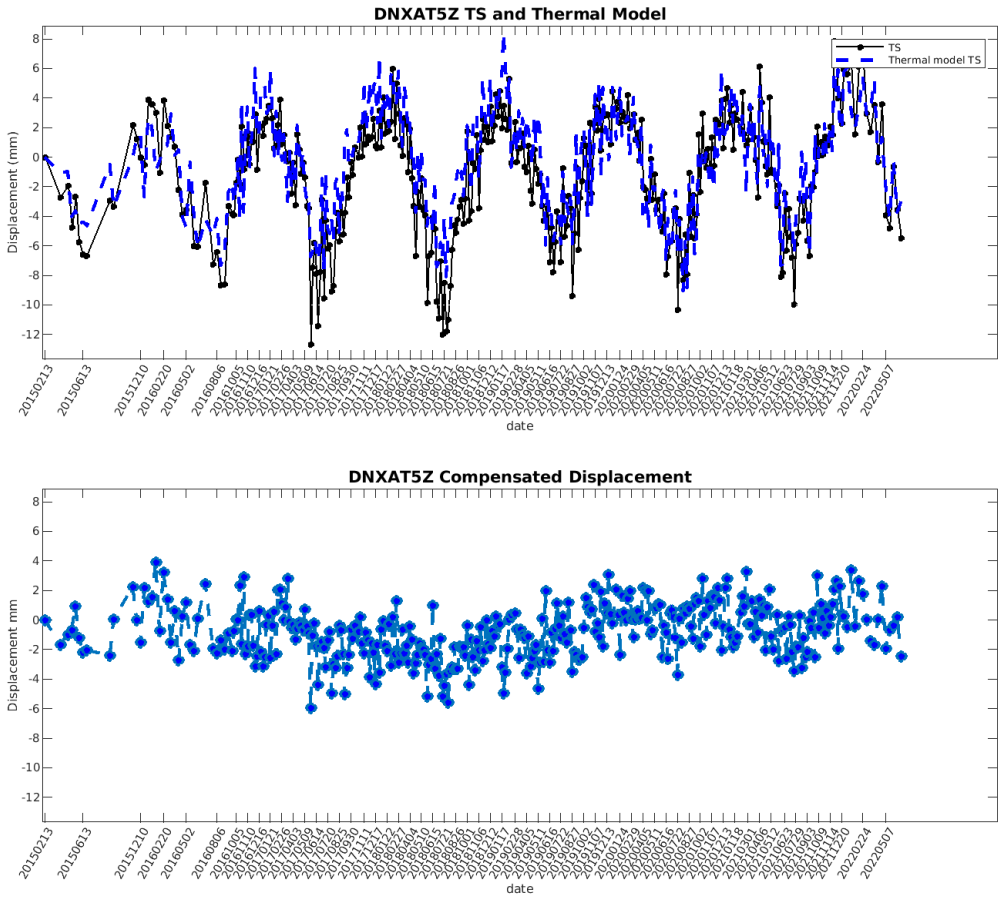

Figure 50: SNT Ascending DNXAT5Z point. Upper: Displacement Time Series in black and its corresponding thermal displacement model in dashed blue. Lower: thermal model compensated displacement Time Series.

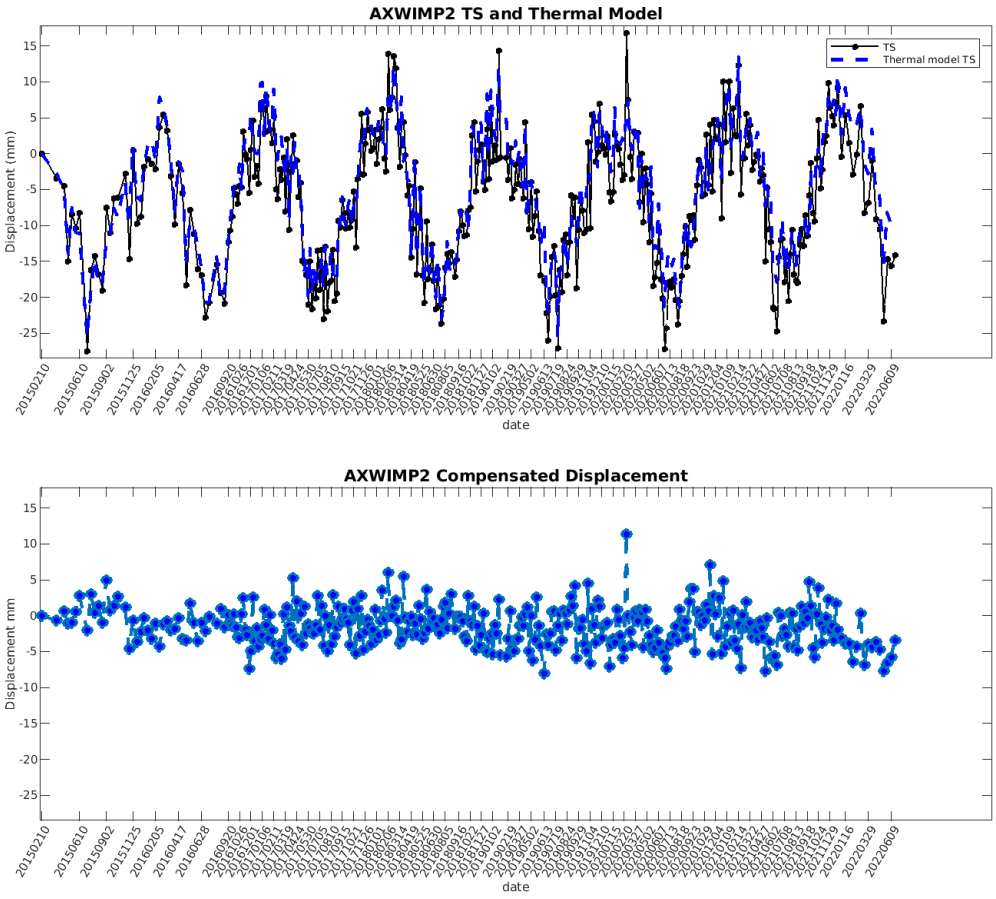

Figure 51: SNT descending AXWIMP2 point. Upper: Displacement Time Series in black and its corresponding thermal displacement model in dashed blue. Lower: thermal model compensated displacement Time Series.

5.6. Alerting system

To characterise the motion behaviour at a bridge component level, a polygon analysis is performed over the point-like SqueeSAR® results. The SqueeSAR® MPs belonging to the bridge's polygons provided by the client are identified, and different statistics are calculated over the values contained in the SqueeSAR® database fields. The mean, the standard deviation, the maximum value, the minimum value, certain percentile, etc., can be calculated considering the displacement and the velocity. This analysis uses the client's shapefiles to achieve a reliable statistical approach. No splitting is performed on arbitrary distance parameters. Furthermore, this avoids the risk of having many empty polygons and thus obtaining a spatially discontinuous appearance for the deformations on the bridges. This approach, complementary to the point-wise analysis, helps to identify better significant episodes among parts of the bridge sharing different structural properties.

An alerting system has been designed by taking advantage of the polygon analysis (with the shapefiles of the bridges provided by the client). The objective is to develop an adaptative alerting system depending on the SqueeSAR® analysis. It is assumed that the seasonality related to temperature variations is part of the normal temporal behaviour of the bridge. The filtered results have been used for the polygon analysis and the alerting system. It is based on the averaged deformation (corresponding to the period of analysis for each satellite) associated with each polygon.

The statistical distribution of each deformation value associated with each polygon is analysed regarding the SqueeSAR® analysis (1929 elements for the SNT solution in descending geometry, 1925 for the SNT solution in ascending geometry, 1097 elements for the 2D decomposition, and 3429 elements for the TSX solution in descending geometry). We assume that the deformation values follow a normal distribution; we consider the statistical distribution example shown in Figure 52.

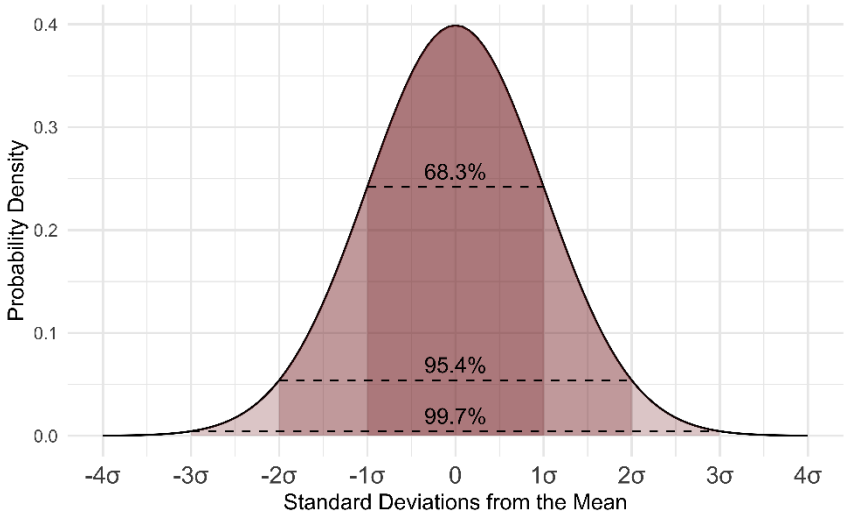

Figure 52: Example of a normal distribution.

For each SqueeSAR® analysis and the averaged deformations d, we consider their mean value m, and their standard deviation σ. The following test t is performed:

$$t = |d - m|$$

If $t < \sigma$, the bridge section represented by the polygon is out of concern.

If $\sigma \leq t < 3\sigma$, the bridge section represented by the polygon is matter of concern.

If $t \geq 3\sigma$, the bridge section represented by the polygon is considered in alert.

The values for all SqueeSAR® analyses are given in the following Table 10.

SqueeSAR® solution	m [mm]	σ [mm]
TSX D	0.23	2.04
SNT A	-3.71	10,49
SNT D	1.65	10.77
SNT EW	3.38	10.40
SNT V	-2.17	10.25

Table 10: Mean and standard deviation values of the deformation associated with the bridge's polygons related to each SqueeSAR® solution.

Figure 53 presents an example of the results with the SNT SqueeSAR® solution in descending geometry over the bridge with index 000789.

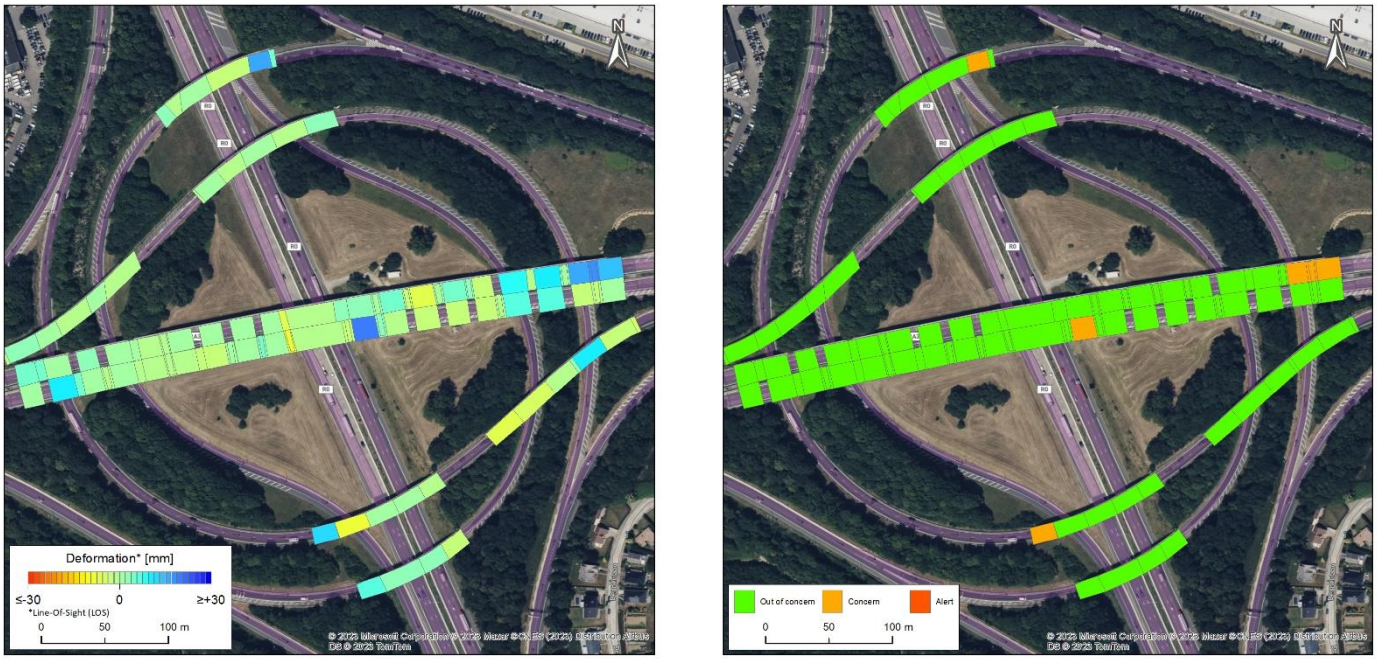

Figure 53: Left: SNT SqueeSAR® deformation [mm] in descending geometry associated with each bridge's polygon. Right: Corresponding alerting system.

6. Monograph

The various products derived from the SqueeSAR® analysis related to each bridge are presented via automated generated monographs. The monographs are composed of several pages, one for each SqueeSAR® solution (TSX in descending geometry, SNT in ascending and descending geometries, SNT 2D decomposition for vertical and horizontal components), and finally, a page with all the deformation profiles. The different elements of the monograph are described below.

- **Deformation**: It is the cumulative displacement for the last date of the SqueeSAR® solution between -30 mm and 30 mm.
- **Standard deviation**: It is the index of the dispersion of the cumulative displacements for each MP, based on the STD_DEF parameter between 0 and 4 mm (see section 2.3).
- **Surroundings**: It is the classification of the MPs based on the analysis of their height estimation classified according to three categories (on the bridge, may be on the bridge, not on the bridge; see section 0).
- **Thermal dilatation constant**: These are the parameters used to correct the temperature component from the time series from different MPs on the bridge between -0.5 mm/°C and +0.5 mm/°C.
- **Polygon analysis**: It represents the different elements of the bridge colour-coded with the cumulative displacement values (for the entire analysis period) extracted from the SqueeSAR® solution between -30 and 30 mm.
- **Alerting system**: It represents the different elements of the bridge colour-coded with the parameters of the warning system (out of concern, concern, alert; see section 0).
- **Deformation profiles**: These represent the deformation profiles for all SqueeSAR® solutions (except the 2D decomposition) with the profile axis and the adaptive size cells (see section 5.3). To plot a deformation profile, cumulative displacement information must be present on two consecutive cells. In this project's scope, it is also chosen to present the cumulative displacements associated with the isolated cells.

7. Comparison of the use of Sentinel-1 and TerraSAR-X images

The objective of this section is to review the impact of using SNT or TSX images in this study for bridge deformation monitoring. The following points are listed below. An important reminder is that the SNT and TSX SqueeSAR® analysis periods are different, about 7.5 years against 2.5 years, respectively.

- **Accuracy**: The acquisition wavelength of SAR images theoretically reaches a millimetre accuracy. The variance of phase observation is proportional to the wavelength of the satellite. When working with different acquisition wavelengths (5.66 cm for C-band data and 3.10 cm for X-band data), it is expected to detect smaller displacements with the smaller acquisition wavelength.
- **Spatial resolution**: The X-band images (TSX) have a higher spatial resolution than C-band images (SNT). The pixel size is about 3x3 m against 20 x 5 m. This results in a higher MP spatial density, ~1 000 MP/km² for SNT, against ~9 500 MP/km² for TSX, which is more suitable for infrastructure monitoring.
- **LOS angle θ**: The LOS angle impacts the comprehension of the results in the case of a 1D study. This angle is lower for the TSX SqueeSAR® (θ = 21.60°) than the SNT SqueeSAR® results (θ = 35.86° for descending geometry, and θ = 40.21° for ascending geometry). It allows an easier direct comparison with the levelling data for the TSX results when the SNT results will need further processing (2D decomposition) to be correctly compared with ancillary data.
- **Atmospheric correction**: As mentioned in section 2.3, a high spatial distribution of the MPs allows a better estimation of the atmospheric contribution and thus reduces the noise level on the estimate of displacements. Furthermore, a lower LOS angle implies a shorter signal passage in the atmospheric layers and, therefore, a lower atmospheric contribution.
- **Data availability**: From an operational perspective, the TSX images are more suitable for deformation monitoring because they are tasked over a dedicated area, a specified period, and an acquisition frequency. ESA manages the SNT image acquisition.

The TSX images are more suitable for infrastructure monitoring because of their sensitivity to small displacements, spatial resolution, and MP spatial density. Moreover, a lower LOS angle allows a faster comparison with ancillary data and a lower atmospheric contribution. From an operational perspective, image acquisition is ensured once they are tasked for monitoring a dedicated area.

However, SNT images allow for assessing a better state of the art of displacement because of availability and free of charge. An analysis with descending and ascending geometry also allows for conducting a decomposition of the true vertical and east-west components of the displacements.

8. Description of the database

SqueeSAR® results are provided in Shapefile format; this database contains several fields described below (Table 11).

Field	Description
Latitude	Latitude of the MP in decimal degrees [°]
Longitude	Longitude of the MP in decimal degrees [°]
CODE	MP Identification Code
HEIGHT	Altitude du PM [m]
H_STDEV	Standard deviation of altitude estimate **HEIGHT** [m]
SRTM_ERR	Difference between the actual MP altitude and the DEM [m]
VEL	Average velocity [mm/yr]. A positive value corresponds to a movement towards the satellite; a negative value corresponds to a movement away from the satellite.
V_STDEV	Standard deviation of average velocity estimate **VEL** [mm/yr]
SEASON_AMP	Estimated amplitude (maximum value) of the sinusoidal model fitted to the time series [mm]
S_AMP_STD	Standard deviation of the amplitude of the sinusoidal model fitted to the time series [mm]
SEASON_PHS	Estimated phase of the sinusoidal model fitted to the time series [rad]
S_PHS_STD	Standard deviation of the phase of the sinusoidal model fitted to the time series [rad]
COHERENCE	Normalised standard deviation (1σ) of the difference between the time series and its model, index [0 1]
STD_DEF	Standard deviation (1σ) of the residuals between the time series and its model [m]
EFF_AERA	Area covered by a group of DS [m²], a value equal to 0 corresponds to a PS
GEO_STDEV	Geolocation uncertainty of the MP [m]
D20XXXXXX	Cumulative displacement at date **D20XXXXXX** [mm]

MEAN_H_BRG	Average height of the bridge estimated from the MPs located within it [m]
STD_H_BRG	Standard deviation of the height of the bridge [m]
SURR_CLASS	Classification of the MP

Table 11. Description of the fields in a SqueeSAR® database.

9. Conclusion

In this project's scope, 457 bridges of different materials, structures or years of construction have been studied. They are within an AOI of 3 126 km² from the south of Brussels to Antwerp (Belgium).

A state-of-the-art deformation has been set using the patented SqueeSAR® algorithm to perform an InSAR analysis over the entire area. Three datasets have been used, including Sentinel-1 (SNT) SAR satellites in ascending and descending geometries and TerraSAR-X (TSX) SAR satellite in descending geometry. The TSX images cover the period from June 20214 to March 2016, and the SNT images cover the period from February 2015 to June 2022. A 2D decomposition (vertical and horizontal components) is carried out using the results from both SNT geometries.

This executive report provides an overview of all SqueeSAR® results and their added values. It includes the following studies:

- an in-depth analysis of zones where no InSAR points are available using amplitude images
- an analysis of surroundings based on the height estimation of the MPs
- automation of longitudinal profiles associated with a bridge sketch
- the detection of sudden changes in displacement
- a temperature variation analysis associated with thermal compensation
- an alerting system based on the different bridge's parts colour-coded with the SqueeSAR® cumulated displacements

TRE ALTAMIRA associates to this technical report 457 monographs correspond to an automated and individual analysis of each bridge for each satellite solution used within this project.

In addition, all SqueeSAR® results and their added values can be downloaded to the TREmaps® visualisation platform.

TRE
ALTAMIRA
A CLS Group Company

TRE ALTAMIRA s.r.l.
Ripa di Porta Ticinese, 79
20143 Milan Italy
Tel: +39 02 4343 121

TRE ALTAMIRA S.L.U.
Carrer de Còrsega, 381-387
08037 Barcelona Spain
Tel.: +34 93 183 57 50

TRE ALTAMIRA Inc.
Suite 410, 475 West Georgia Street
Vancouver, BC V6B 4M9 Canada
Tel: +1 604 331 2512

tre-altamira.com